PLASTIC DEFORMATION OF CIRCULAR METAL DIAPHRAGMS

A THESIS

By

TAPAN KUMAR PAUL

Submitted to the Department of Mechanical Engineering, Bangladesh University of Engineering & Technology Dhaka in partial fulfilment of requirements for the Degree of

MASTER OF SCIENCE

IN

ENGINEERING (MECHANICAL)

November, 1983

CERTIFICATE OF RESEARCH

Certified that the work presented in this thesis is the result of the investigation carried out by the candidate under the supervision of Dr. M.F. Ilahi at the Department of Mechanical Engineering, BUET, Dhaka.

Tapankumarpaul

Candidate

MF Ilahi

Supervisor

DECLARATION

I do hereby declare that neither this thesis nor any part thereof has been submitted or is being concurrently submitted in candidature for any degree at any other university except for publication.

Tapankumar Paul
Candidate

PLASTIC DEFORMATION OF CIRCULAR METAL DIAPHRAGMS

A THESIS

By

TAPAN KUMAR PAUL

Approved as to style and content by:

(DR. M.F. ILAHI) : Chairman
Associate Professor,
Mechanical Engg. Dept.,
BUET, Dhaka.

(DR. ~~AZIZUL HUQ~~) : Member
Professor and Head,
Dept. of Mech. Engg.,
BUET, Dhaka.

(DR. M. WAHHAJUDDIN) : Member
Assistant Professor,
Dept. of Mech. Engg.,
BUET, Dhaka.

(DR. MOHIUDDIN CHOWDHURY) : Member
Associate Professor,
Dept. of Naval Arch. & Marine Engg.
BUET, Dhaka.

(DR. FASIHUDDIN MAHTAB) : Member
Director,
Prokoushali Sangsad Ltd.,
131, Motijheel C/A,
Dhaka.

November, 1983

ABSTRACT

The hydrostatic plastic forming of a metal diaphragm has been considered from the theoretical point of view. Hydrostatic bulging of diaphragm is of great value since the work-hardening characteristics of materials can be obtained upto large plastic strains. Woo's general method of solution using incremental strains has been chosen since this appears to be the most straight forward approach for a circular diaphragm. In his paper Woo presented numerical results only for a total strain theory since this reduced computer time. Also there was some difficulty in satisfying the boundary condition $\varepsilon_\theta = 0$, at the clamped edge (when using incremental strain theory). In the present work, the computational method of Ilahi et al.(14) has been followed as it does not suffer from later difficulties. The analysis is carried out for the case of commercial purity soft aluminium and soft 70/30 brass diaphragms of 10 inch diameter. In this theoretical analysis the material has been assumed to possess anisotropy in the thickness direction i.e normal anisotropy.

For the last thirty years the anisotropic yield criterion of Hill (17) has been used to analyse different forming processes including balanced biaxial tension of sheet metals. The predicted values based on this criterion, did not agree very closely with the experimental results for all values of anisotropy, but had

limited success. Recently Hill proposed a new anisotropic yield criterion which introduces an additional parameter 'm' dependent on the material property. Some studies show that the agreement between experiment and the new theory is better.

It is found that the correlation between the present theoretical results based on the new yield criterion and the experimental results obtained by Ilahi (10) is very good. This indicates that the latest theory of yielding for anisotropic material proposed by Hill may be successful in predicting the actual behaviour of anisotropic materials under large strains.

ACKNOWLEDGEMENT

The author wishes to express his gratitude, profound respect and indebtedness to his teacher and guide Dr. M.F. Ilahi, Associate Professor, Dept. of Mechanical Engineering, Bangladesh University of Engineering & Technology, Dhaka, for the whole-hearted help, unfailing interest, and fruitful criticism in carrying out this thesis work to completion.

He is also grateful to Dr. Anwar Hossain, Prof. and former Head, Dept. of Mech. Engg., BUET, Dhaka for his kind help and inspiration in continuing this study and also to his teacher Dr. Azizul Huq, Professor and Head and Dr. S.M. Nazrul Islam, Associate Professor, Dept. of Mech. Engg., BUET, Dhaka, for giving inspiration in carrying out the programme.

Author would like to give thanks to the staff of the Computer Centre, BUET for the help given while obtaining the theoretical results.

Thanks are also to Bangladesh University of Engg. and Technology for financial help.

CONTENTS

LIST OF FIGURES

LIST OF TABLES

NOTATION

Roman Letters

$f(\sigma_{i,j})$	*plastic potential*
y	*vertical height of a generic point*
n	*work-hardening index*
p	*hydrostatic pressure*
Δp	*a small increment in pressure*
$(r_o)_i, (r_o)_{i+1} \ldots$	*initial radii of particular elements of material*
$(r)_i, (r)_{i+1} \ldots$	*current radii of elements of initial radii,* $(r_o)_i, (r_o)_{i+1}$
R_a	*radius of diaphragm, Fig. 3.1.1*
R	*R-value-, strain ratio in uniaxial tension*
t_o	*initial thickness of material*
$(t)_i, (t)_{i+1} \ldots$	*current thicknesses of elements of initial radii,* $(r_o)_i, (r_o)_{i+1} \ldots$
F, G, H, L, M, N	*parameters dependent on the current state of anisotropy*
w_o, w	*original and current width of a tensile specimen*
K	*constant in the empirical equation,* $\sigma = K\bar{\varepsilon}^n$
R_o, R_{45}, R_{90}	*strain ratios along 0, 45 and 90 degrees to the rolling direction*
X, Y, Z	*tensile yield stresses along x, y, z directions*
h	*polar height*

Greek Letters

τ_{xy}, τ_{yz}, τ_{zx}	shear stresses
ε_θ , ε_r	natural circumferential and radial strain
ε_x, ε_y, ε_z	natural strains along x, y, z directions
ε_t, ε_w	natural strain along thickness and width direction
ε_m, ε_o	maximum thickness strain, polar thickness strain
$d\varepsilon_x$, $d\varepsilon_y$, $d\varepsilon_z$	natural strain increments along x, y and z directions
$d\varepsilon_t$, $d\varepsilon_w$	natural strain increments along thickness and width directions
$\bar{\varepsilon}$, $d\bar{\varepsilon}$	generalized strain and strain increment
θ	bulge profile angle
ρ_1, ρ_2	radii of curvature of bulge profile
σ	generalized stress
λ	a parameter
$d\lambda$	constant multiplier in Hill's equations
ξ	$= r_o/a$
Ψ	auxiliary angle (angular position of stress vector in deviatoric plane

Subscripts

o	initial state
θ, r, t	cylindrical co-ordinates, circumferential radial and thickness direction respectively
x, y, z	cartesian co-ordinates

CHAPTER I

INTRODUCTION

The circular hydrostatic bulge test is often used in the studies of sheet metal forming to obtain the work hardening characteristics of materials upto large plastic strains. Considerable attention has been paid to the deformation of a circular metal diaphragm under uniform lateral pressure. This gives rise to a biaxial tensile stress and it is one of the best methods of investigating plastic flow in sheet metal. This deformation process has been related to diaphragms subjected to underwater explosion and to the design of safety diaphragms or bursting discs of pressure vessels.

Several theories have been put forward to predict the stress and strain distribution, the shape of the diaphragm and the plastic unstable condition. Most of the analysis are based on yield criterion for isotropic materials and used total strain theory. Only a few are based on the anisotropic yield function and used incremental strain theory.

1.1 Literature Review

Hill (1) developed a more general theoretical model for small strains based on Von-Mises theory, but his method of successive approximation is only valid for sufficiently work hardened materials. Of greater practical interest is a special solution obtained by Hill on the assumption that the typical section of the bulge and particle flow path form a bipolar co-ordinate system. He put forward a simple expression which relates the polar thickness strain with hardening exponent at instability. $\varepsilon_m = \frac{4}{11}(2n + 1)$ clearly shows the superiority of diaphragm test in determining the work hardening characteristics of materials at large strain values.

Woo (2) has described an iterative method of solution to determine the stress and strain distribution for axisymmetric problems in plane stress. Basically the solution was obtained by successive approximation of stresses and strains according to work hardening characteristics of material, the geometry of the process and plasticity theory. The stresses and strains so determined are correct when the equilibrium equation and boundary condition are satisfied. In his paper he extended the general method of analysis for the axisymmetric forming process to the case of hydrostatic bulging of circular diaphragms. He used total strain theory in numerical solution since it reduced computer time. Also there was some difficulty (when using incremental strain theory) in attaining the boundary condition $\varepsilon_\theta \approx o$, at the clamped edge.

In the appendix of their paper Chakrabarty and Alexander (3) gave the governing equations and the boundary conditions. According to the boundary conditions, either ψ(angle between stress vector and line of pure shear) or $\bar{\dot{\varepsilon}}$ (generalized strain rate) at the edge must be zero. In obtaining a numerical solution it was difficult to satisfy the two point mixed boundary conditions.

Bramley and Mellor (4) carried out experiments to assess the degree of anisotropy in stabilized sheet steels. The measured R-values were used to predict the plastic flow behaviour at the centre of a circular diaphragm subjected to fluid pressure. The macroscopic theory of anisotropic plastic flow (Hill (17)) gave some qualitative agreement with experimental results. For the simple case of plastic flow at the centre of a circular diaphragm they found that taking an average R-value (from the equation $\bar{R} = 1/4(R_0 + 2R_{45} + R_{90})$) was a satisfactory approach. Because the average $\bar{R}$ value calculated from the area under the experimental curve was not widely different from that was calculated from the above formula.

Bramley and Mellor (5) made an attempt to predict the deformation behaviour of titanium and zinc sheet when subjected to a biaxial stress system in the plane of the sheet. Correlation between theory and experiment was good for titanium but was poor for zinc.

Wang and Shammamy (6) analysed hydrostatic bulging of a circular sheet clamped at the periphery, based on incremental strain theory and the total strain theory. The material of the sheet was assumed to have strain hardening capacity and to be anisotropic in thickness direction. They found that as the polar strain was increased, pressure reached a maximum and then decreased, whereas the total strain theory gave unsatisfactory results. They found that the differential equations associated with total strain theory, possessed singularity which had the effect of restricting the range of calculation to a certain value of polar strain.

Pearce (7) determined stress and strain curves of various sheet metals in uniaxial and balanced biaxial tension. He concluded that Hill's (17) theory of yielding satisfactorily predicts the plastic behaviour of materials whose anisotropy is described with $\bar{R} > 1$, but fail to predict the same for the materials $\bar{R} < 1$.

It is evident that from the previous works anisotropic plasticity theory does not hold good for all materials. One of these is aluminium. The anomalous behaviour of aluminium sheet was further studied by Woodthorpe and Pearce (8) for the case of circular diaphragm. Correlation between theory and experiment confirmed the previous findings.

Yamada and Yokouchi (9) studied the hydrostatic forming of axisymmetric diaphragms using incremental strain theory. They assumed the material to be incompressible and anisotropic in thickness direction only. Their simple boundary condition is that circumferential strain at the edge is zero. They formulated 8 equations with 9 unknowns and suggested the use of pressure as a parameter for solving the equations. Two equations, one for circumferential stress distribution and other for meridional strain distribution, gave rise to some problems. They extrapolated the results to obtain meridional strain at the edge. The expression for circumferential stress contains square root term which sometimes becomes zero during subsequent stages. However they gave a complete solution for the diaphragm problem. But the stress ratio (σ_θ/σ_r) obtained by them at the edge is not acceptable. The correct ratio is ½(for a isotropic material) and R/R+1 (for anisotropic materials). This was the main drawback of their diaphragm theory.

Ilahi (10) studied the diaphragm problem both experimentally and theoretically. He showed that the theoretical predictions based on Hill's original theory for the case of soft aluminium and soft 70/30 brass, which have $\bar{R}$ value less than unity, does not give satisfactory correlation with experimental values. Moreover he also used Yamada and Yokouchis' anisotropic diaphragm theory and shows that the results are underestimated in comparison with the result obtained by Woo's theory.

Parmar and Mellor (11) studied the plastic expansion of a circular hole in sheet metal, subjected to biaxial stress to predict the plastic stress and strain distribution with the new yield function proposed by Hill (12). The theoretical predictions show good correlation with experimental strain distributions for sheets of aluminium killed steel, soft 70/30 brass and soft aluminium. They concluded that the new yield function has greater generality than his original criterion. In their work no attempt was made experimentally to determine the value of the parameter m in yield function. Instead the values of m which gave the best fit between theoretical and experimentalresults were determined. It is thought that this approach is justified if, for a given strain level, the theoretical curves follow the experimental results closely over the range from simple tension to balanced biaxial tension and provided good correlation persists at different strain levels. They showed that for aluminium killed steel m = 2, for soft 70/30 brass m = 1.82 and for soft aluminium m = 1.7 gave good correlation between theory and experiment.

Hill and Storakers (13) studied further the mechanics of bulge test on a clamped sheet for small deflections. They assumed material to be isotropic and considered both creep and time independent plasticity. They did not compare their results with any experimental values.

Ilahi et al. (14) presented a numerical method of solution for the plastic deformation of a circular diaphragm. The analysis was applied to the bulging of soft commercial purity aluminium sheet. Woo's general method of solution was adopted since this appeared to be the most straight forward approach for a circular diaphragm. The analysis was based on the new anisotropic yield function of Hill which was of the same form as used by Parmar and Mellor (11). Woo presented numerical results only for a total strain theory since it reduced computer time but also because there was some difficulty in using incremental strain theory in satisfying the boundary conditions $\varepsilon_\theta \simeq o$, at the edge. The computational method of Ilahi et al. overcomes this later difficulty. For this soft aluminium ($\bar{R} < 1$),results were correlated with the experiment, it was shown that the correlation was good for pressure, strain and geometrical relationships.

Chater and Neale (15,16) used finite element method to compare results for diaphragm from flow theory and deformation theory. They also considered the [illegible] strain-rate effects and strain-rate independent behaviour but did not compare their theoretical results with any experimental results.

1.2 Plan for the Present Work

Experimental results of diaphragm test (obtained by Ilahi (10)) for two materials, soft commercial purity aluminium and soft 70/30 brass are available.

The objective of the present work is to predict the plastic flow behaviour of the above two materials, by applying the new yield function. Thus the work mainly deals with the numerical solution of a modified diaphragm theory for predicting different variables of the deformation process.

Correlation between the theoretical results and the experimental results will be made to see whether the latest yield function can predict the actual behaviour of the above two materials or not. For generating the theoretical results, IBM 370/115 computer will be used.

CHAPTER II

ANISOTROPY IN SHEET METAL AND HILL'S THEORY

2.1 Anisotropy in sheet metals

Previously, theoretical analysis of sheet metals assumed that the materials were isotropic i.e, the crystal grains are randomly distributed and the strength is independent of the direction. But during deformation process this random distribution no longer exists. The distribution of the grains has one or more maxima. If such a maximum is well defined it is referred to as a preferred orientation. If the orientation of the individual crystals are not random, the yield stress and the macroscopic stress and strain relations vary with directions, this phenomenon is termed as anisotropy. Anisotropy can be due to mechanical fibring, inclusions, porosity etc.. Plastic anisotropy—flow stress, work hardening behaviour—which results from crystallographic preferred orientation, giving the metal a 'texture' can be varied in a sheet metal by altering the sequence and nature of the thermal and mechanical treatments which are used in manufacture.

However measurements of the changes in width strain and thickness strain during uniaxial plastic deformation will indicate anisotropy, and their ratio $R = d\varepsilon_w/d\varepsilon_z$ is called the strain ratio or commonly R value.

Variation of R with direction of testing in the sheet plane is termed planar anisotropy, ΔR. For isotropic materials, $R = 1$ and $\Delta R = 0$. The value of R in a biaxial situation is defined by Pearce (7) as

$$\bar{R} = (1/4)(R_o + 2\ R_{45} + R_{90})$$

or some variant on this respect depending on the number of directions in which tests are made. Bramley and Mellor (4) showed that the $\bar{R}$ value determined from the area under the experimental curve was not widely different from that obtained from the above formula and pointed out that the above formula for $\bar{R}$ may be successfully used.

2.2 Hill's Original and New Theory of Yielding and its Application to Sheet Metal Study

To study the deformation of anisotropic sheet metals, Hill's macroscopic anisotropic theory of yielding has been widely used. This theory is similar to that based on the Von-Mises yield criterion and its associated flow rule of isotropic materials.

Hill (17) extended the concept of plastic potential to anisotropic materials which has the following quadratic form.

$$2f(\sigma_{i,j}) = F(\sigma_y - \sigma_z)^2 + G(\sigma_z - \sigma_x)^2 + H(\sigma_x - \sigma_y)^2 + 2L\tau_{yz}^2 + 2M\tau_{zx}^2 + 2N\tau_{xy}^2 = 1 \qquad (1)$$

where F, G, H, L, M, and N are constants dependent on the current state of anisotropy.

For load in the plane of the sheet ($\tau_{yz} = \tau_{zx} = 0$) along the principal axes of anisotropy ($\tau_{xy} = 0$) eqn. (1) reduces to

$$F(\sigma_y - \sigma_z)^2 + G(\sigma_z - \sigma_x)^2 + H(\sigma_x - \sigma_y)^2 = 1 \qquad (2)$$

For plane stress ($\sigma_z = 0$) and considering planar isotropy ($R_0 = R_{45} = R_{90} = \bar{R}$) eqn. (2) may further be reduced to the form

$$2(1+R)Y^2 = (1+2R)(\sigma_x - \sigma_y)^2 + (\sigma_x + \sigma_y)^2 \qquad (3)$$

where Y is the uniaxial yield stress in the plane of the sheet. In cylindrical co-ordinates

$$2(1+R)Y^2 = (1+2R)|\sigma_\theta - \sigma_r|^2 + |\sigma_\theta + \sigma_r|^2 \qquad (4)$$

(Mode sign is used since $\sigma_\theta \gtrless \sigma_r$).

Its associated flow rule from the standard normality hypothesis

$$\frac{d\varepsilon_r}{-1(1+2R)|\sigma_\theta - \sigma_r| + |\sigma_\theta + \sigma_r|} = \frac{d\varepsilon_\theta}{(1+2R)|\sigma_\theta - \sigma_r| + |\sigma_\theta + \sigma_r|} = \frac{d\varepsilon_t}{2|\sigma_\theta + \sigma_r|}$$

Generalized stress from eqn.(4)

$$\bar{\sigma} = \{(1/2(1+R))|(1+2R)|\sigma_\theta - \sigma_r|^2 + |\sigma_\theta + \sigma_r|^2|\}^{\frac{1}{2}}$$

and generalized strain increment

$$d\bar{\varepsilon} = \frac{1+R}{\sqrt{(1+2R)}}(d\varepsilon_r^2 + \frac{2R}{1+R} d\varepsilon_r \, d\varepsilon_\theta + d\varepsilon_\theta^2)^{\frac{1}{2}}$$

For the last thirty years this anisotropic yield criterion of Hill has been used to analyse different forming processes including balanced biaxial tension of sheet metals. The predicted values based on this criterion, did not agree very closely with the experimental results for all values of anisotropy, but had limited success. Recently Hill (12) proposed a new yield criterion for deformation under normal anisotropy which introduces a new parameter 'm' dependent on the material property.

The newly proposed criterion is expressed as follows:

$$2(1+R)Y^m = (1+2R)|\sigma_\theta - \sigma_r|^m + |\sigma_\theta + \sigma_r|^m \qquad (5)$$

where Y is the uniaxial yield stress in the plane of the sheet and m is an index, greater than or equal to one. When $m = 2$ the equation reduces to Hill's original yield criterion for normal anisotropy (eqn. 4). When $m = 2$ and $R = 1$ the equation reduces to the Von-Mises expression for yielding under plane stress for isotropic materials. The yield locus must be convex and this is satisfied provided $m \geqslant 1$. When $m < 2$ the locus is elongated in the direction of balanced biaxial tension. Normal anisotropy is now defined by two parameters R and m.

Associated flow rule:

The flow rule associated with the above new yield function by the standard normality hypothesis is given by

$$\frac{d\varepsilon_\theta}{(1+2R)\frac{|\sigma_\theta - \sigma_r|^m}{(\sigma_\theta - \sigma_r)} + \frac{|\sigma_\theta + \sigma_r|^m}{(\sigma_\theta + \sigma_r)}} = \frac{d\varepsilon_r}{-(1+2R)\frac{|\sigma_\theta - \sigma_r|^m}{(\sigma_\theta - \sigma_r)} + \frac{|\sigma_\theta + \sigma_r|^m}{(\sigma_\theta + \sigma_r)}}$$

$$= -\frac{d\varepsilon_t}{\frac{2|\sigma_\theta + \sigma_r|^m}{(\sigma_\theta + \sigma_r)}} = \frac{d\bar{\varepsilon}}{2(1+R)\bar{\sigma}^{m-1}} \qquad (6)$$

where $d\varepsilon_\theta$, $d\varepsilon_r$ and $d\varepsilon_t$ are the increment of circumferential, meridional and thickness strains respectively. $\bar{\sigma}$ is the generalised stress which is defined from the new yield function as

$$\bar{\sigma} = \left\{ \frac{1}{2(1+R)} \left[(1+2R)|\sigma_\theta - \sigma_r|^m + |\sigma_\theta + \sigma_r|^m \right] \right\}^{1/m} \qquad (7)$$

and generalised strain increment based on the work equivalence hypothesis is expressed as

$$d\bar{\varepsilon} = \frac{[2(1+R)]^{1/m}}{2} \left[\frac{1}{(1+2R)^{1/(m-1)}} |d\varepsilon_\theta - d\varepsilon_r|^{m/(m-1)} \right.$$

$$\left. + |d\varepsilon_\theta + d\varepsilon_r|^{m/(m-1)} \right]^{\frac{m-1}{m}} \qquad (8)$$

CHAPTER III

DIAPHRAGM THEORY AND NUMERICAL SOLUTION

3.1 Diaphragm Theory

Modified diaphragm theory (based on Woo's general theory of axisymmetric forming process) as adopted by Ilahi et al (14) has been followed. Theoretical formulations are given here.

Equilibrium Equations:

From figure 3.1.1, equilibrium in meridional direction gives

$$\frac{d(t\sigma_r)}{dr} = \frac{(\sigma_\theta - \sigma_r)t}{r} \qquad (1)$$

Where t is the current thickness, r is the current radius and σ_θ and σ_r are the circumferential and meridional stress components respectively.

For Equilibrium of Vertical Forces:

$$\frac{P}{t} = \frac{2\sigma_r \, \mathrm{Sin}\,\theta}{r} \qquad (2)$$

where P is the hydrostatic pressure and θ is the bulge profile angle.

Equilibrium of Forces in the Direction of P:

$$\frac{P}{t} = \frac{\sigma_\theta}{\rho_2} + \frac{\sigma_r}{\rho_1} \qquad (3)$$

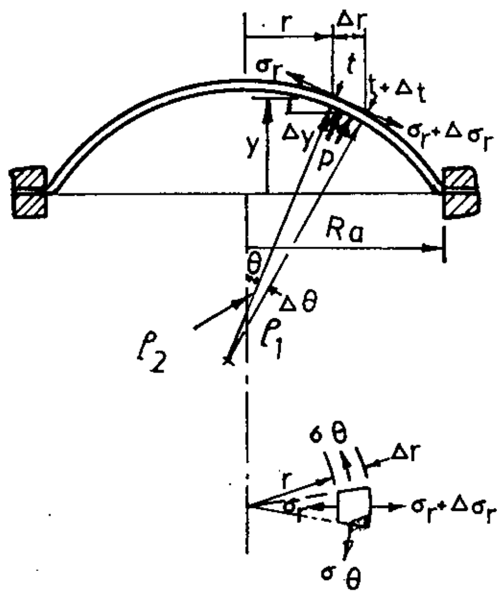

FIG. 3.1.1 Hydrostatic bulging–stresses in an element

Where ρ_1 and ρ_2 are the meridional and circumferential radii of curvature respectively.

Yield Function:

The new yield function for normal anisotropy as described in Art. 2.2 is

$$2(1+R)Y^m = (1+2R)|\sigma_\theta - \sigma_r|^m + |\sigma_\theta + \sigma_r|^m \tag{4}$$

Associated Flowrule:

$$\frac{d\varepsilon_\theta}{(1+2R)\dfrac{|\sigma_\theta - \sigma_r|^m}{(\sigma_\theta - \sigma_r)} + \dfrac{|\sigma_\theta - \sigma_r|^m}{(\sigma_\theta + \sigma_r)}} = \frac{d\varepsilon_r}{-(1+2R)\dfrac{|\sigma_\theta - \sigma_r|^m}{(\sigma_\theta - \sigma_r)} + \dfrac{|\sigma_\theta + \sigma_r|^m}{(\sigma_\theta + \sigma_r)}}$$

$$= -\frac{d\varepsilon_t}{2|\sigma_\theta + \sigma_r|^m} = \frac{d\bar{\varepsilon}}{2(1+R)\bar{\sigma}^{m-1}} \tag{5}$$

Where $d\varepsilon_\theta$, $d\varepsilon_r$ and $d\varepsilon_t$ are the increments of circumferential, meridional and thickness strains respectively. $\bar{\sigma}$ is the generalised stress which is found from the yield function as

$$\bar{\sigma} = \left\{\frac{1}{2(1+R)}\left[(1+2R)|\sigma_\theta - \sigma_r|^m + |\sigma_\theta + \sigma_r|^m\right]\right\}^{1/m} \tag{6}$$

Generalised Strain Increment:

$$d\bar{\varepsilon} = \frac{[2(1+R)]^{1/m}}{2} \left[\frac{1}{(1+2R)^{1/(m-1)}} \left| d\varepsilon_\theta - d\varepsilon_r \right|^{m/(m-1)} + \left| d\varepsilon_\theta + d\varepsilon_r \right|^{m/(m-1)} \right]^{\frac{m-1}{m}} \tag{7}$$

Work hardening characteristics is expressed with the following empirical equation:

$$\bar{\sigma} = K\bar{\varepsilon}^{\,n} \tag{8}$$

Where K and n are constants for the material.

The strain increments are written from the flow rule (5) as

$$d\varepsilon_\theta = \left[(1+2R) \frac{|\sigma_\theta - \sigma_r|^m}{(\sigma_\theta - \sigma_r)} + (\sigma_\theta + \sigma_r)^{m-1} \right] \frac{d\bar{\varepsilon}}{2(1+R)\bar{\sigma}^{m-1}} \tag{9}$$

$$d\varepsilon_r = \left[-(1+2R) \frac{|\sigma_\theta - \sigma_r|^m}{(\sigma_\theta - \sigma_r)} + (\sigma_\theta + \sigma_r)^{m-1} \right] \frac{d\bar{\varepsilon}}{2(1+R)\bar{\sigma}^{m-1}} \tag{10}$$

and $$d\varepsilon_t = -(\sigma_\theta + \sigma_r)^{m-1} \frac{d\bar{\varepsilon}}{(1+R)\bar{\sigma}^{m-1}} \tag{11}$$

The above equations are valid for all values of σ_θ and σ_r for both σ_θ and $\sigma_r > 0$. From equation (9) and (11) the stress components can be derived in terms of strain increments to give

$$(\sigma_\theta + \sigma_r) = \bar{\sigma} \left[- (1+R) \frac{d\varepsilon_t}{d\bar{\varepsilon}}\right]^{1/(m-1)} \qquad (12)$$

$$\text{and } (\sigma_\theta - \sigma_r) = \bar{\sigma} \left[\frac{2(1+R)}{(1+2R)} \frac{(d\varepsilon_\theta + d\varepsilon_t/2)}{d\bar{\varepsilon}}\right]^{1/(m-1)} \quad \text{when } d\varepsilon_\theta > d\varepsilon_r$$

$$(13)$$

$$\text{or } (\sigma_r - \sigma_\theta) = \bar{\sigma} \left[\left|\frac{2(1+R)}{(1+2R)}\right| \frac{|d\varepsilon_\theta + d\varepsilon_t/2|}{d\bar{\varepsilon}}\right]^{1/(m-1)} \quad \text{when } d\varepsilon_\theta < d\varepsilon_r$$

Solving eqns. (12) and (13) expression for σ_θ and σ_r in terms of strain increments can be found.

Due to the axial symmetry of the deformation, the relation between ε_θ and ε_t can be deduced from the consideration of volume constancy of an elemental ring. If t_o is the initial thickness, $(r_o)_i$ and $(r_o)_{i+1}$ are the initial radii of an elemental ring, then reffering to Fig. 3.1.1,it follows that

$$\pi((r_o)^2_{i+1} - (r_o)^2_i) \; to = X. \left(\frac{t_i + t_{i+1}}{2} \right)$$

where X is the area between the current radii r_i and r_{i+1} and the material thickness t_i and t_{i+1} at r_i and r_{i+1} respectively. The area X depends on the profile of the deformed metal which may vary during the forming process as in the case of hydrostatic bulging. The above equation may be written in the form as

$$\pi[(r_o)^2_{i+1} - (r_o)^2_i]\ t_o = 2\pi\left[\frac{(\rho_1)_i + (\rho_1)_{i+1}}{2} + \frac{t_i + t_{i+1}}{4}\right]$$

$$\times\left[\frac{(\rho_2)_i + (\rho_2)_{i+1}}{2} + \frac{t_i + t_{i+1}}{4}\right]$$

$$\times[\mathrm{Cos}(\theta)_i - \mathrm{Cos}(\theta)_{i+1}]\ [(t_i + t_{i+1})/2] \qquad (14)$$

Where ρ_1 and ρ_2 are the radii of curvature.

3.2 Numerical Solution

The unknowns are σ_θ, σ_r, $\bar{\sigma}$, ρ_1, ρ_2, ε_θ, ε_t, $\bar{\varepsilon}$, θ and P. The unknowns are found from the above equations (1) to (3),(7), (8) and (12) to (14) by considering (ε_t) pole as a monotonic increasing quantity and with the approximation of P, provided the following initial and boundary conditions are satisfied.

(i) Initial conditions along the radius of the bulge,

$$\sigma_r = \sigma_\theta = \varepsilon_\theta = \varepsilon_t = 0,\ t = t_o \text{ and } P = 0$$

(ii) Boundary conditions

At the pole, (r = 0) $\quad \sigma_r = \sigma_\theta$, $\varepsilon_\theta = -\varepsilon_t/2$, $\rho_1 = \rho_2$ and $\theta = 0$

At the edge $r = R_a$ $\quad$ Circumferential strain $\varepsilon_\theta \simeq 0$ at all stages of deformation.

The numerical method followed is same as that of Ilahi et al (14). The method of solution is presented in the Appendix-1. When satisfactory results for a stage is found the height distribution is found from the equation

$$\frac{dy}{dr_o} = - \sin\theta \quad e^{\varepsilon_r} \qquad (a)$$

Where y is the height of the bulge at an angle θ measured from the pole. Equation (a) is integrated using a finite difference form, starting with the condition at the fixed edge $r = R_a$, $y = 0$.

3.3 Computer Programming

A computer programme was developed in Fortran IV language, and was run on IBM 370/115 computer. The programme was developed for a 10 inch diaphragm i.e, $R_a = 5$ inch. The initial radii interval were set out 0.1 inch apart,from the first radius near to the pole which was 0.5. Hence corresponding to each assumed incremental pressure, stresses and strains at 47 points were computed. For each point the condition for meridional equilibrium $(t\sigma_r)/(t\sigma_r)' = 1 \pm 0.00003$ was set to be satisfied. For a particular stage the solution was considered satisfactory when the condition at the fixed edge was $\varepsilon_\theta \leqslant 0.0003$. $(-\varepsilon_t)_{pole}$ was increased in steps of 0.02.

The algorithm and the flow chart for the programme are given in the Appendix-II and Appendix-III respectively. Computer programme in Fortran IV is presented in the Appendix-IV.

3.4 Material Properties

In correlating the theoretical results with the experimental results, the experimental values of diaphragm test of Ilahi (10) are taken. The uniaxial tensile test data and empirical expression for work hardening characteristics for the two materials (soft aluminium and soft 70/30 brass) are taken from Ilahi (10) and Parmar and Mellor (11). Because these two materials for the present analysis are the same with those were considered by them.

The measured R values are:

For soft aluminium: $R_{0^o} = 0.620$, $R_{45^o} = 0.581$ and $R_{90^o} = 0.756$

$\bar{R}$ (as in Art. 2.1) = 0.635

work hardening characteristics

$\bar{\sigma} = 19166\ \bar{\varepsilon}^{0.269}$ lbf/in^2

thickness of the sheet t_o = 0.0349 inch

For soft 70/30 brass: $R_{0^o} = 0.817$, $R_{45^o} = 0.90$, $R_{90^o} = 0.827$

$\bar{R} = 0.86$

work-hardening characteristics

$\bar{\sigma} = 115330\ (0.042 + \bar{\varepsilon})^{0.624}$ lbf/in^2

$\bar{\varepsilon} \leqslant 0.111$

$\bar{\sigma} = 109240\bar{\varepsilon}^{0.51}$ lbf/in^2

$\bar{\varepsilon} > 0.111$

thickness of the sheet t_o = 0.0376 inch

It may be mentioned here that at the point $\bar{\varepsilon}$= 0.111, the two expressions for soft 70/30 brass predict a little different values which is not detrimental to the final solution.

The value of the parameter m in the yield function are taken from Parmar and Mellor (11).

For soft aluminimum = 1.7

For soft 70/30 brass m = 1.82

these work hardening expressions and $\bar{R}$ values were used by Parmar and Mellor (11) to predict the strain distribution in an annulus of the same aluminium and soft 70/30 brass sheets subjected to a radial tension at its outer periphery. Correlation between theory and experiment showed that m = 1.7 for soft aluminium and m $\doteq$ 1.82 for soft 70/30 brass were required to give the best fit between theoretical and experimental results.

CHAPTER IV

RESULTS AND CONCLUSIONS

4.1 Theoretical Results and Comparison with Experiment

The theoretical results for the two materials (soft aluminium and soft 70/30 brass) obtained by numerical solution of the theory in the section 3.2 have been plotted and compared with the experimental results obtained by Ilahi (10).

The comparison of the results for soft aluminium are shown in Figs.4.1.3 to 4.1.11. The results for soft 70/30 brass are shown in Figs.4.1.12 to 4.1.20. The theoretical results based on the assumption that m = 2 have also been presented in the figures.

In case of soft aluminium, the maximum pressure obtained is 124.49 lbf/in^2 which almost agrees with the experimental value. Computation beyond the maximum pressure gives reduction in pressure, this is in contrast to the finite element formulation obtained by Kobayashi and Kim (18) where the solution diverged at a point which they associated with pressure maximum.

4.2 Discussion

Soft aluminium

Condition at the pole: The relation between the pressure and polar thickness strain is shown in Fig. 4.1.3. The correlation is very good with the experimental results when the analysis is based on $m = 1.7$ rather than the theory based on the assumption $m = 2$. Between plane strain tension and balanced biaxial tension a value $m = 2$ under estimates the yield stress of aluminium sheet and therefore it is to be expected that the theoretical values of the forming pressure will be too low as evident from the figure.

The relation between the polar radius of curvature and polar thickness strain is shown in Fig. 4.1.4. Almost all the experimental points lie on the theoretical curve, the agreement was better than the old theory ($m = 2$).

Fig. 4.1.5 shows the relationship between polar height and polar thickness strain. The correlation is found quite satisfactory than that obtained by theory $m = 2$. Fig. 4.1.6 and 4.1.7 shows the relationship between polar radius of curvature and polar height, pressure and polar height respectively and the correlation is better than the old theory, $m = 2$. The values of polar heights for a particular polar radius of curvature $\rho=10$ in. from experiment, predicted by old and new theory are 1.35, 1.425 and 1.35 respectively. Experimental value almost coincides with the value obtained by new theory,value obtained by old theory deviates 5.56% from the experimental one.

From the pressure vs. polar height curve, for a particular polar height $h = 1.133$, the value of pressure obtained by old theory and new theory deviates 25% and 10.9% (upto polar height y $\doteq$ 1.48) from the experimental value respectively. The values of pressure obtained by new theory almost coincide with experimental values when polar height is greater than 1.75 in. This may be due to the epxression for work hardening characteristics.

Conditions along the meridian:

The distribution of circumferential strain and thickness strain, along the meridian, are shown in Figs. 4.1.8 and 4.1.9 respectively. The correlation with the experimental result is very good, when the value of the index m is 1.7. The meridional strain distribution is satisfactory at lower strain level but the data are scattered at higher values of strain as shown in Fig..Fig. 4.1.11 shows the distribution of height which correlates very satisfactorily with experimental results and demonstrates the superiority of the new theory over the old one.

Soft 70/30 brass

Conditions at the pole: Fig. 4.1.12 shows the relationship between pressure and thickness strain. The curve obtained from the new theory, m = 1.82 correlates with the experimental results better than the old theory m = 2, upto the pressure 661 psi. Beyond 661 psi, the solution becomes divergent and did not agree with the experimental value. From the previous works of Ilahi et. al (14), Kobayashi and Kim (18),when using incremental strain theory, the solution diverged at a point where they noticed, the pressure is maximum. They also pointed out that this rigid plastic formulation ,the theoretical results were valid only upto the maximum pressure. Pressure 661 psi which is close to the fracture pressure 670 psi as obtained by Ilahi (10).

The relation between the polar height and polar thickness strain is shown in Fig. 4.1.13. The agreement between the experiment and theoretical results (m = 1.82) is good and it is seen that for a given polar height m = 2 predicts too much thinning at the pole of the bulge.

Curves of polar radius of curvature against polar thickness strain are given in Fig. 4.1.14. Again it is clear that there is good correlation between experiment and the theoretical prediction based on m = 1.82.

Polar height versus the polar radius of curvature curves are shown in Fig. 4.1.15 where the prediction is better with the new theory m = 1.82 than with the old theory.

The relation between polar height and pressure is shown in Fig. 4.1.16. Here the correlation is quite satisfactory.

Conditions along the meridian:

The distribution of the circumferential strain along the meridian for different stages of deformation is shown in Fig. 4.1.17. In the numerical solution the polar strain is one of the independent variables. The circumferential strain distribution is shown for some given values of polar thickness strain. Here the correlation is satisfactory. The discrepency between Hill's original (m = 2) and new theory (m = 1.82) becomes less. From the Fig. 4.1.17 it is evident that the circumferential strain depends on the geometry of the diaphragm than the yield function.

Fig. 4.1.18 shows the distribution of thickness strain across the diaphragm. The theoretical curves have been compared with some of the experimental curves for the same polar thickness strain. The correlation between experiment and the new theory (m = 1.82) is very satisfactory. Near the pole and also away from pole the correlation is found very good but the original theory (m = 2) is unsatisfactory for predicting the values well away from the pole. Fig. 4.1.18 demonstrates that the thickness strain distribution is much dependent on the yield function of the material and m = 1.82 is appropriate to this soft brass sheet and leads to a more uniform distribution of the thickness strain.

Curves for meridional strain distribution across the diaphragm are shown in Fig. 4.1.19. The distribution found in this case is not good. Throughout the diaphragm for low strain level the correlation is good but it is found unsatisfactory at higher strain values.

Fig. 4.1.20 gives the distribution of height throughout the diaphragm at different polar thickness strains. The correlation between the experimental and theoretical results are very satisfactory. The theoretical results are underestimated in relation to the experimental results when the prediction is based on $m = 2$. The values of heights at a particular position across the diaphragm, $r/a = 0.3$, from experiment, the old and new theory are 2.61, 2.4 and 2.6 respectively. Experimental value almost coincides with the value obtained by the new theory; value obtained by old theory deviates 8.04% from the epxerimental value.

4.3 Conclusions

This theoretical analysis, based on Hill's new yield function for anisotropic materials with values of $m = 1.82$ for soft 70/30 brass and $m = 1.7$ for soft aluminium gives results for a deforming diaphragm which satisfactorily agree with the experimental results. The pressure for a particular polar thickness strain is better predicted with the new theory and is underestimated significantly when plastic yielding is based on Hill's original theory (assuming $m = 2$).

Polar height versus polar thickness strain, polar radius of curvature versus polar thickness strain, pressure versus polar height and polar height versus polar radius of curvature are in good agreement with the existing experimental results when the analysis is based on the new theory.

Circumferential strain and particularly thickness strain distribution across the diaphragm (thickness strain distribution is very dependent on the yield function as evident from the analysis) can be accurately predicted with the new theory.

Only the prediction of meridional strain distribution along the diaphragm, except at lower strain level, (upto $(-\varepsilon_t)_{pole} = 0.22$) is not satisfactory. Value of m may change with strain level.

Height distribution across the diaphragm (when predicted by the new theory) is in good agreement with the existing experimental results when compared with the agreement based on original theory.

It may be concluded here that all the deformation parameters can be accurately predicted for balanced biaxial tension and plane stress tension by using Hill's new yield function in case of bulging of circular diaphragms in sheet metal study. The new yield function is more general than his original yield function for anisotropic materials.

The most direct method of checking the yield function is of course, to determine experimental yield loci at various strain levels. This is particularly difficult in the case of sheet metals. More experimental work and corresponding theoretical analysis are needed to study further the applicability of the new theory to different deformation processes for other materials of different anisotropy.

Pressure $p(lb_f/in^2)$	Polar thickness $t(in)$	polar thickness strain $-(\varepsilon_t)_{pole}$	Polar radius of curvature $\rho(in)$	Polar hoop stress $\sigma_\theta(lb_f/in^2)$	Polar height $h(in)$	Stress ratio at the edge σ_θ/σ_r
0	0.0376	0		0	0	
67.26	0.0368	-0.02	23.075	21056.17	0.566	0.5099
154.16	0.0351	-0.06	13.260	28864.33	1.029	0.5442
233.42	0.0340	-0.100	10.365	35556.68	1.360	0.5411
307.41	0.0326	-0.14	8.900	41851.69	1.634	0.5509
375.01	0.0314	-0.18	7.968	47574.80	1.874	0.5472
433.40	0.0301	-0.22	7.338	52701.55	2.086	0.5470
483.30	0.0289	-0.26	6.885	57388.43	2.278	0.5487
525.68	0.0278	-0.30	6.542	61733.33	2.455	0.5337
561.79	0.0267	-0.34	6.269	65802.43	2.620	0.5382
592.12	0.0257	-0.38	6.048	69642.93	2.776	0.5398
617.34	0.0247	-0.42	5.865	73289.93	2.922	0.5418
637.88	0.0237	-0.46	5.713	76770.37	3.060	0.5396
654.73	0.0228	-0.50	5.580	80105.50	3.191	0.5372
661.83	0.0223	-0.52	5.520	81723.94	3.253	0.5383

Table 4.1.1 Theoretical results for soft 70/30 brass diaphragm of 10 inch diameter.

Pressure $p(lb_f/in^2)$	Polar thickness $t(in)$	Polar thickness strain $-(\varepsilon_t)_{pole}$	Polar radius of curvature $\rho(in)$	Polar hoop stress $\sigma_\theta(lb_f/in^2)$	Polar height $h(in)$	Stress ratio at the edge σ_θ/σ_r
21.00	0.0342	-0.02	21.905	6723.50	0.566	0.5437
46.14	0.0328	-0.06	12.872	9035.26	1.046	0.4708
64.09	0.0315	-0.10	10.214	10366.15	1.349	0.5559
78.07	0.0303	-0.14	8.820	11348.17	1.598	0.5154
89.09	0.0291	-0.18	7.945	12141.88	1.813	0.5300
97.80	0.0280	-0.22	7.339	12815.31	2.003	0.5127
104.77	0.0269	-0.26	6.885	13404.34	2.176	0.5203
110.26	0.0258	-0.30	6.532	13930.39	2.335	0.5244
114.56	0.0248	-0.34	6.248	14407.40	2.482	0.5260
117.88	0.0238	-0.38	6.010	14844.97	2.620	0.6407
120.38	0.0229	-0.42	5.809	15250.06	2.750	0.4757
122.18	0.0220	-0.46	5.635	15627.85	2.872	0.6246
123.48	0.0211	-0.50	5.479	15982.34	2.982	0.4284
124.13	0.0203	-0.54	5.346	16316.67	3.078	0.8980
*124.48	0.0195	-0.58	5.221	16633.35	3.169	0.4097
124.48	0.0187	-0.62	5.107	16934.45	3.254	0.0859
124.33	0.0180	-0.66	4.996	17221.66	3.334	0.0380

Table 4.1.2 Theoretical results for soft aluminium diaphragm of 10 inch diameter.
* The solution is valid only upto the maximum pressure 124.48.

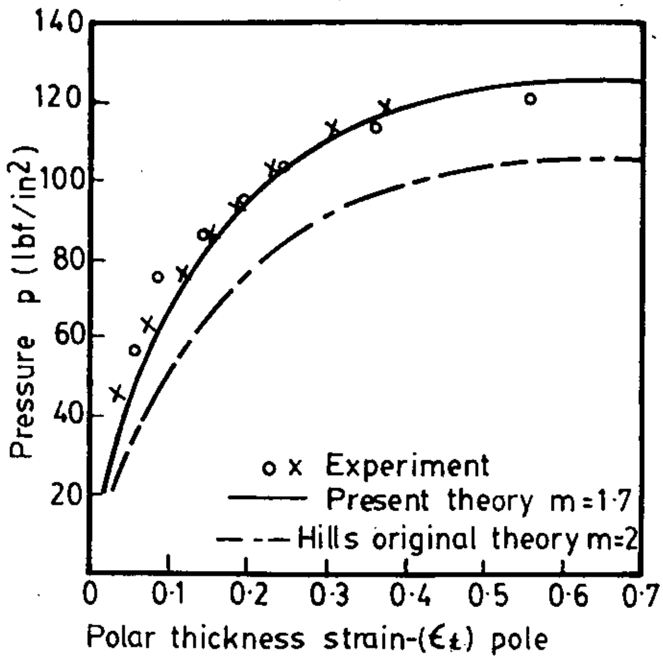

FIG. 4·1·3 PRESSURE V·s. POLAR THICKNESS STRAIN - SOFT ALUMINIUM
Comparison of theoretical results with experimental results.

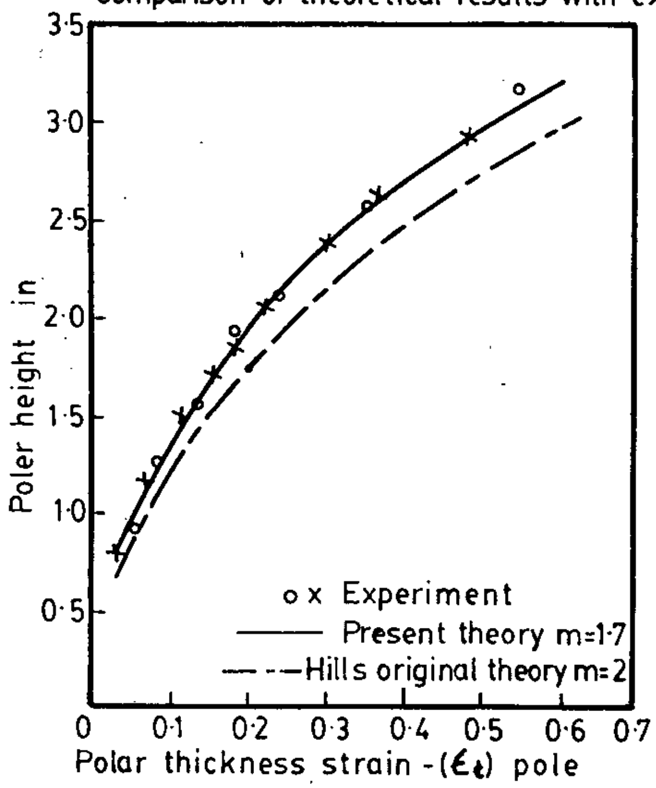

POLAR HEIGHT VS. POLAR THICKNESS STRAINS
Comparison of theoretical results with the experimental results
FIG. 4·1·5

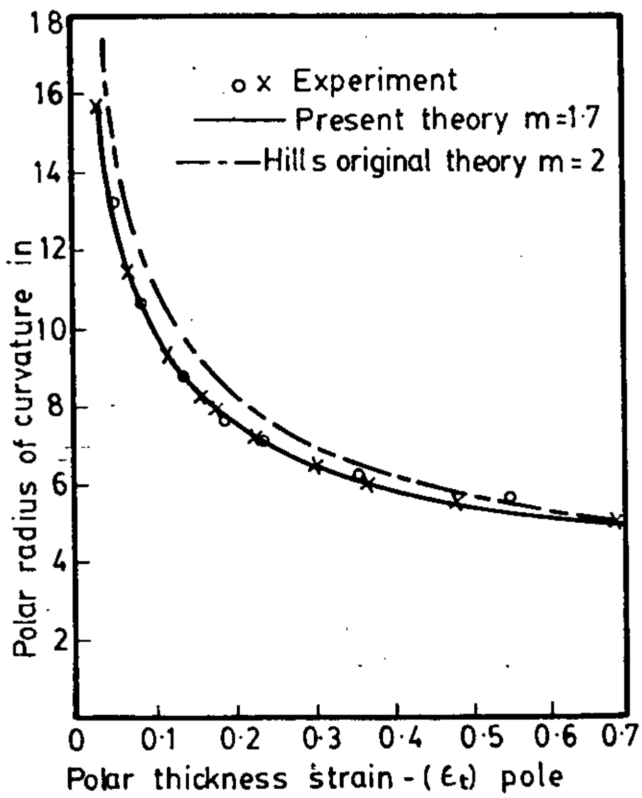

POLAR RADIUS VS. POLAR THICKNESS STRAIN-SOFT ALUMINIUM

Comparison of theoretical results with experimental results

FIG·4·1·4

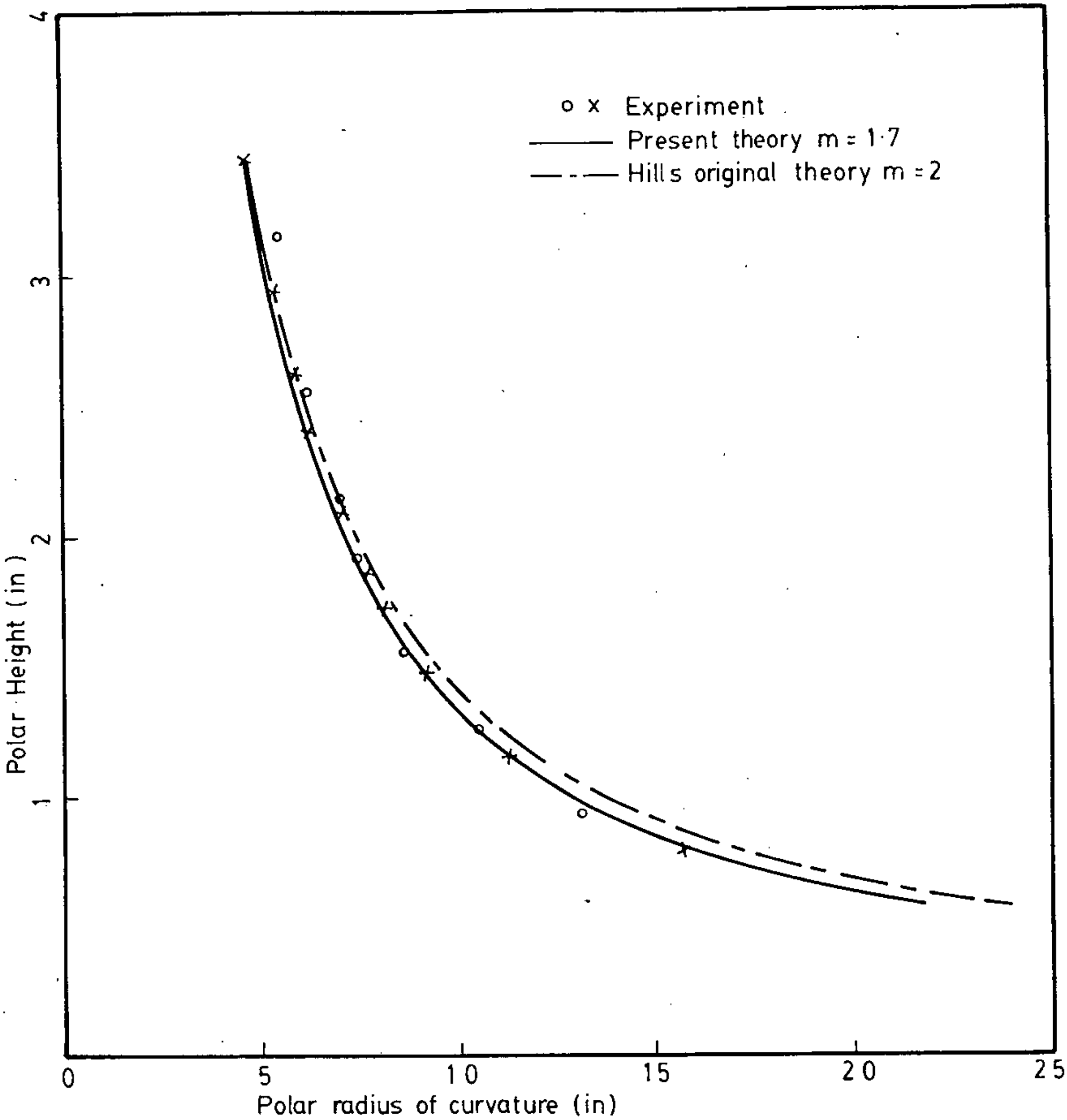

POLAR HEIGHT VS· RADIUS OF CURVATURE–SOFT ALUMINIUM
Comparison of experimental results with theoretical results
FIG·4·1·6

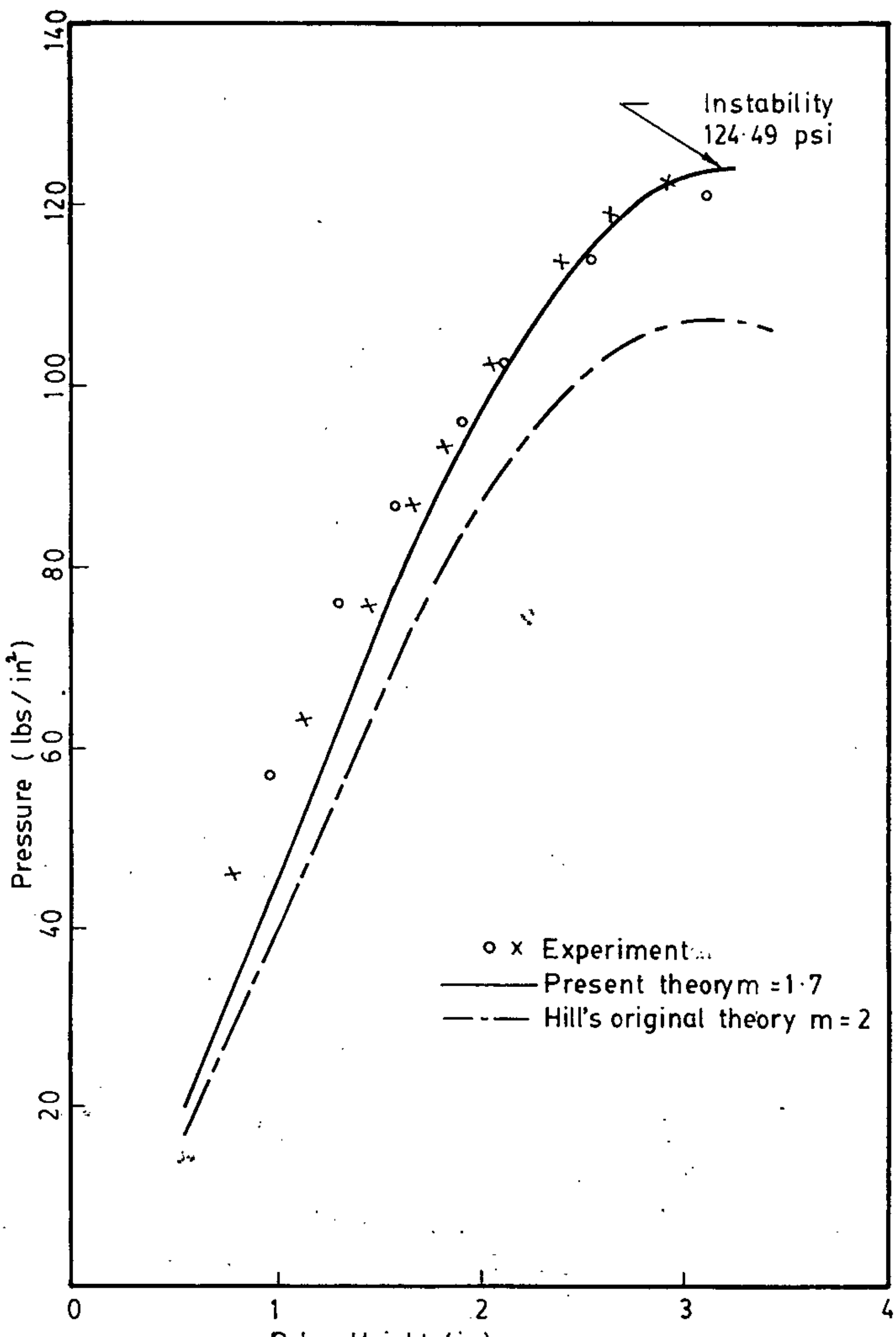

PRESSURE VS. HEIGHT-SOFT ALUMINIUM
Comparison of theoretical results with experimental results
FIG·4·1·7

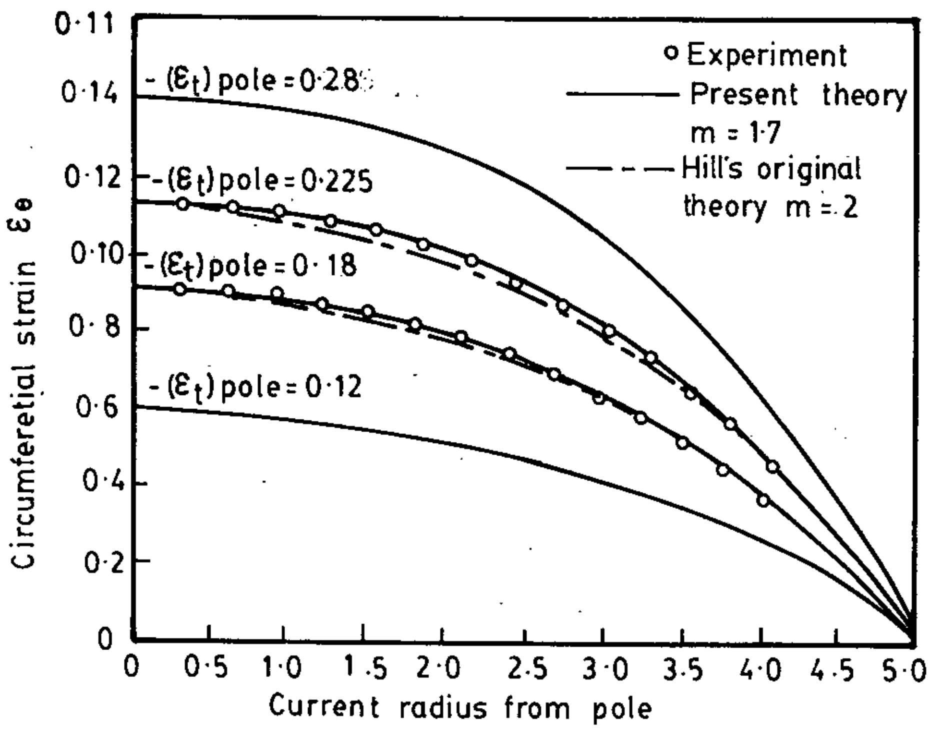

CIRCUMFERENTIAL STRAIN DISTRIBUTION

Comparison of theoretical results with experimental results

FIG. 4·1·8

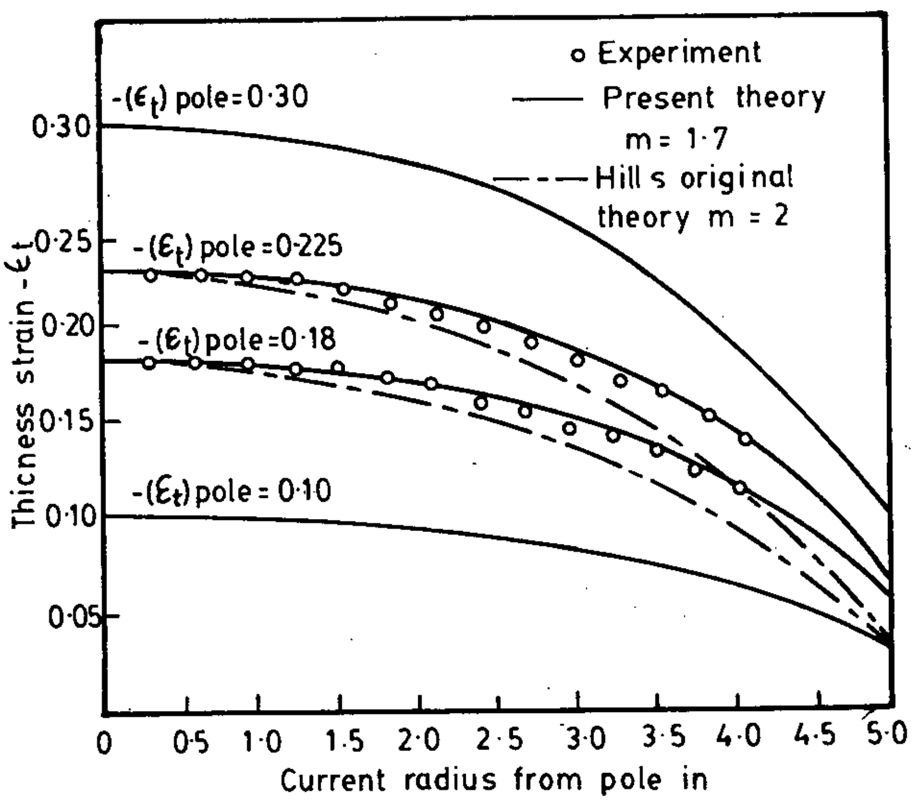

THICKNESS STRAIN DISTRIBUTION

Comparison of theoretical results with experimental results

FIG. 4.19

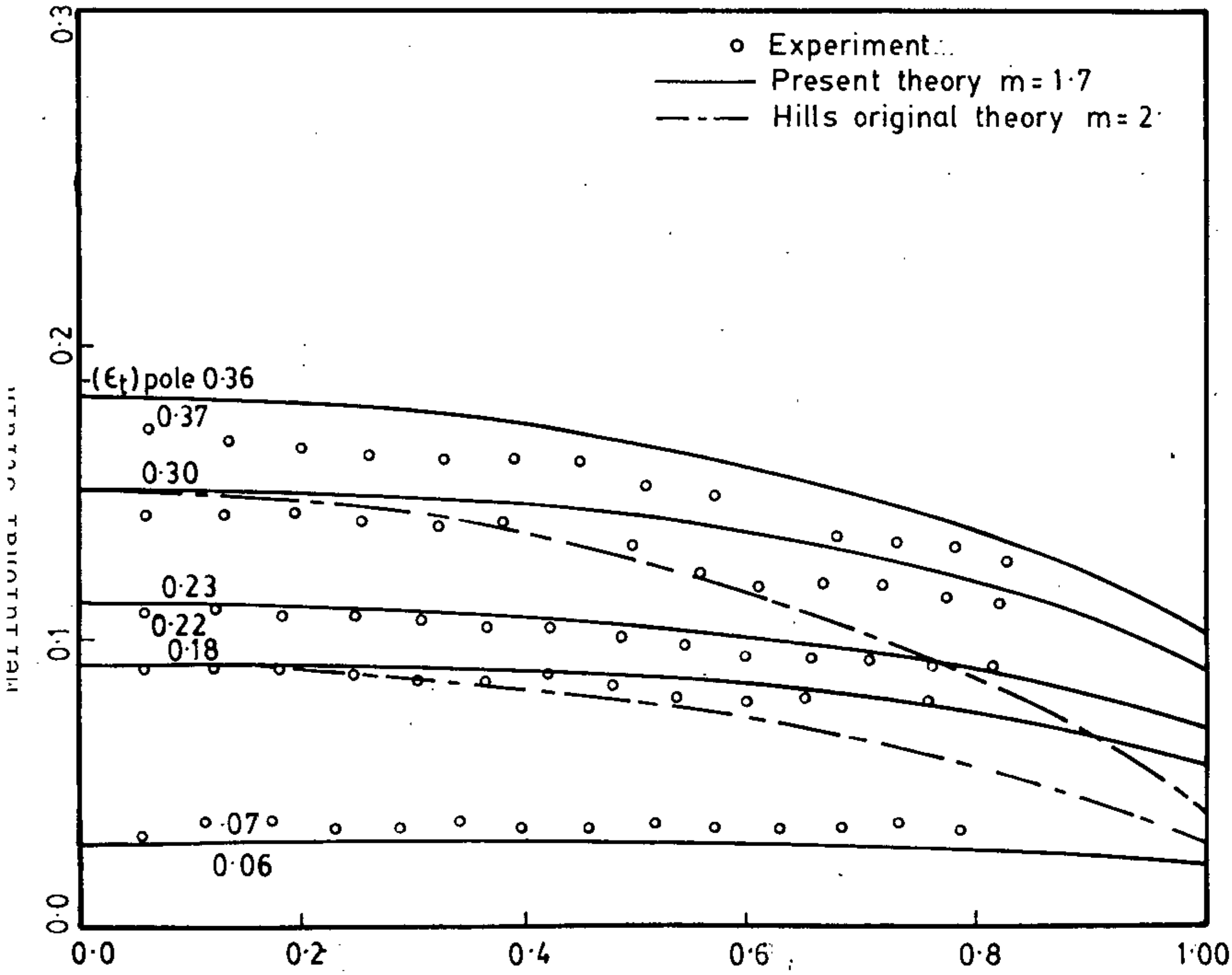

MERIDIONAL STRAIN DISTRIBUTION–SOFT ALUMINIUM

Comparison of theoretical results with experimental results

FIG. 4.1.10

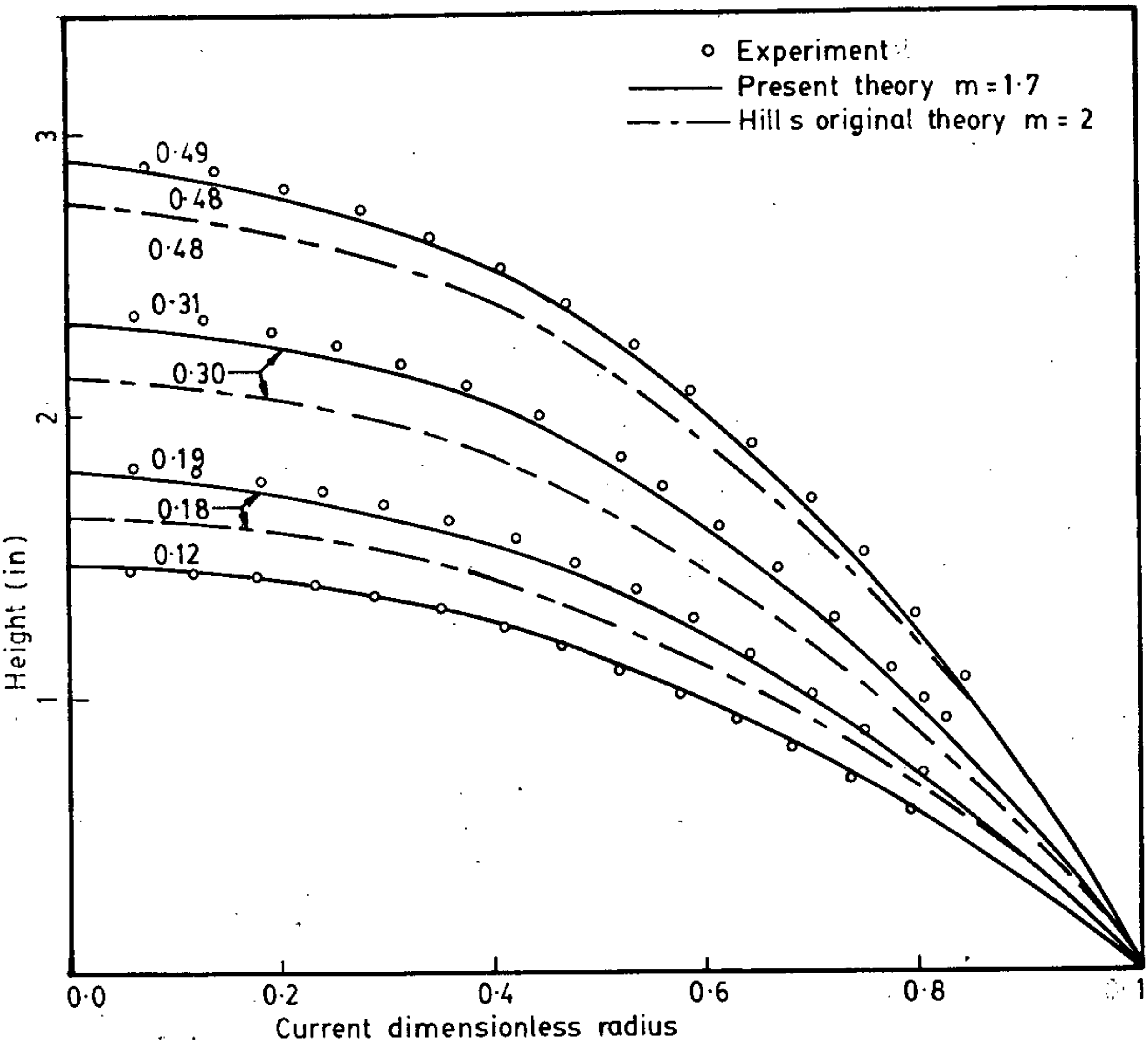

HEIGHT DISTRIBUTION-SOFT ALUMINIUM
Comparison of theoretical results with experimental results
FIG· 4·1·11

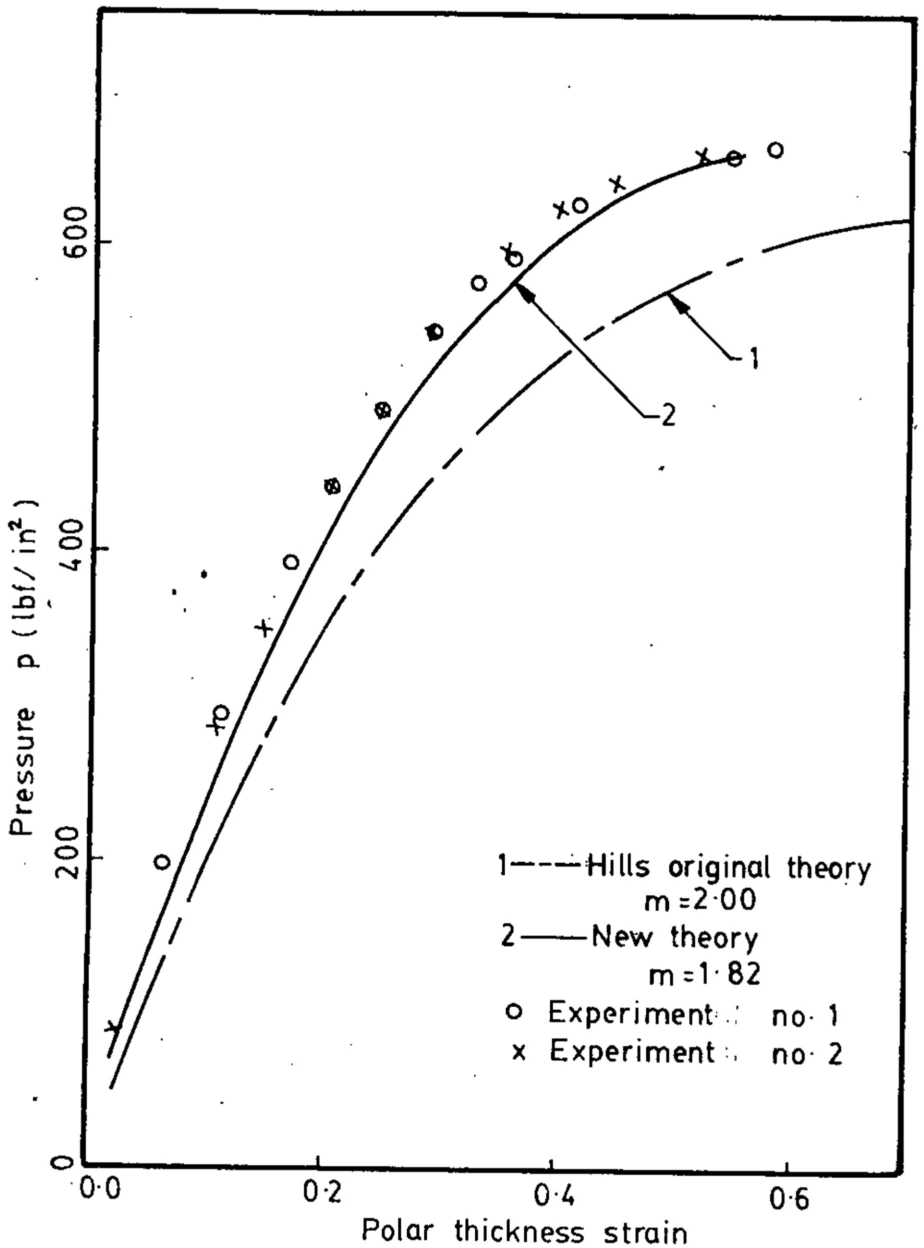

FIG·4·1·12 Theoretical and experimental variation of hydrostatic pressure with polar thickness strain for soft 70/30 brass

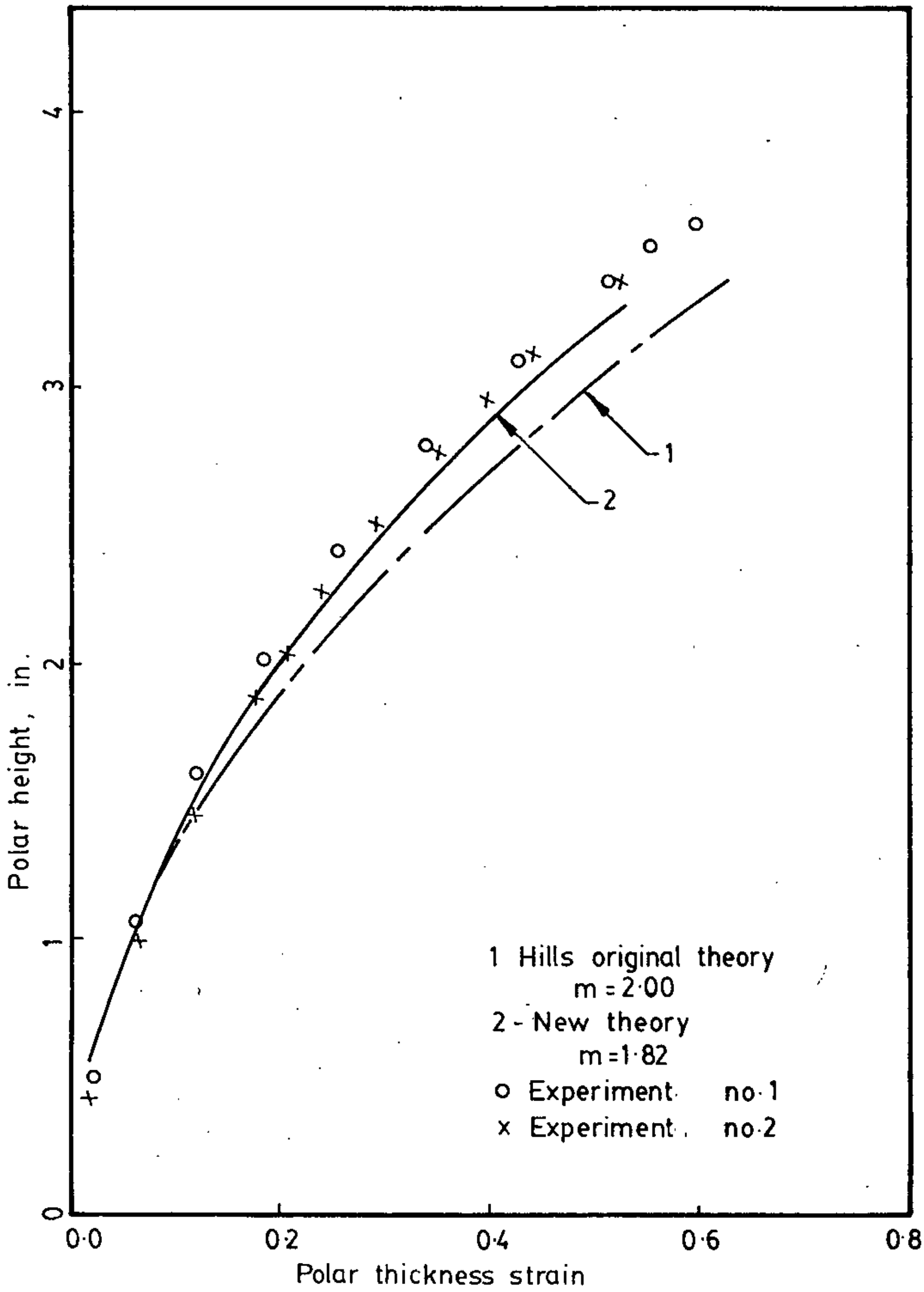

FIG·4·1·13 Theoretical and experimental variation of polar height with polar thickness strain for soft 70/30 brass

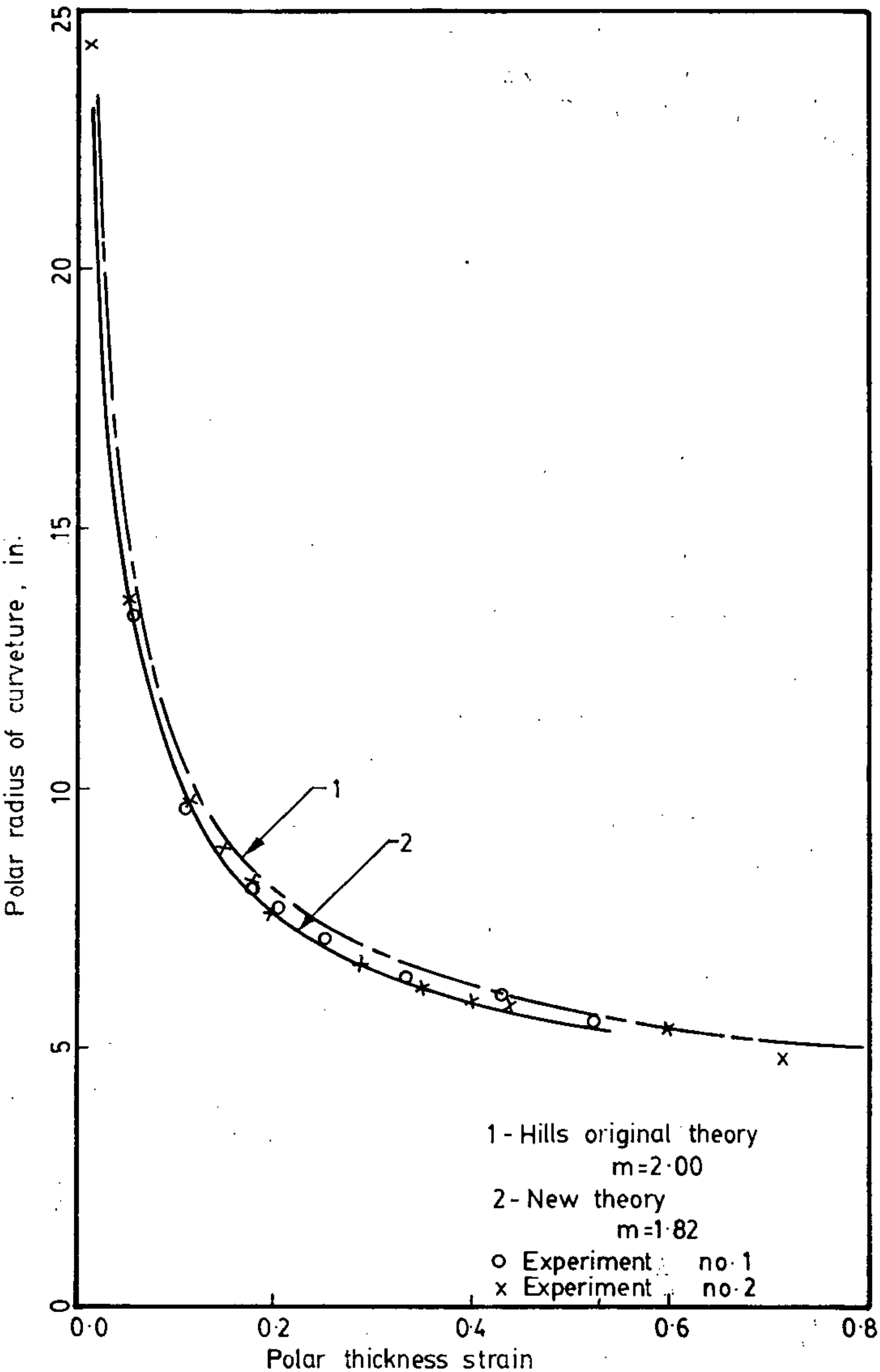

FIG·4·1·14 Theoretical and experimental variation of polar radius of curvature with polar thickness strain for soft 70/30 brass

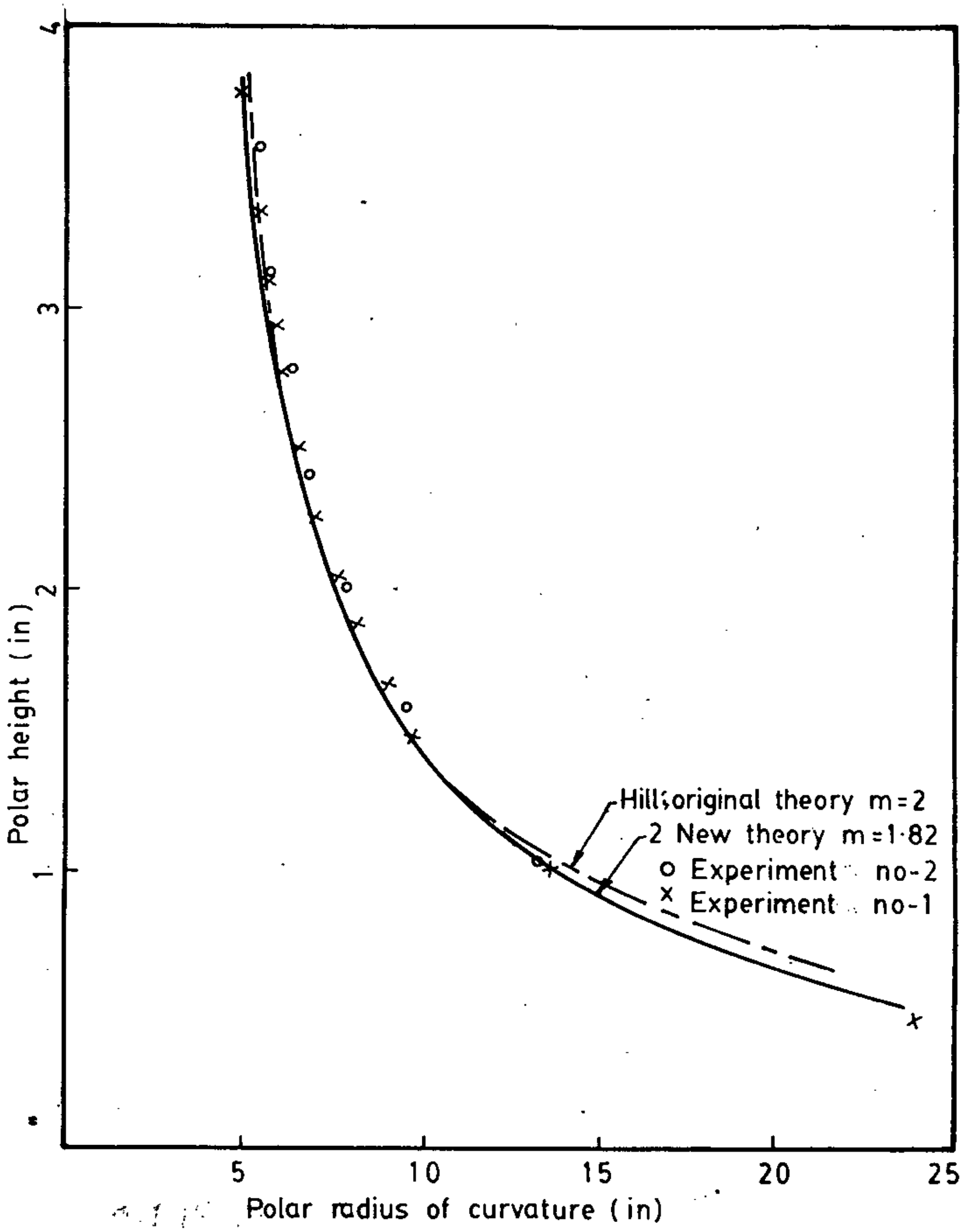

POLAR HEIGHT VS. RADIUS OF CURVATURE—SOFT BRASS
Comparison of theoretical results with the experimental results
FIG. 4.1.15

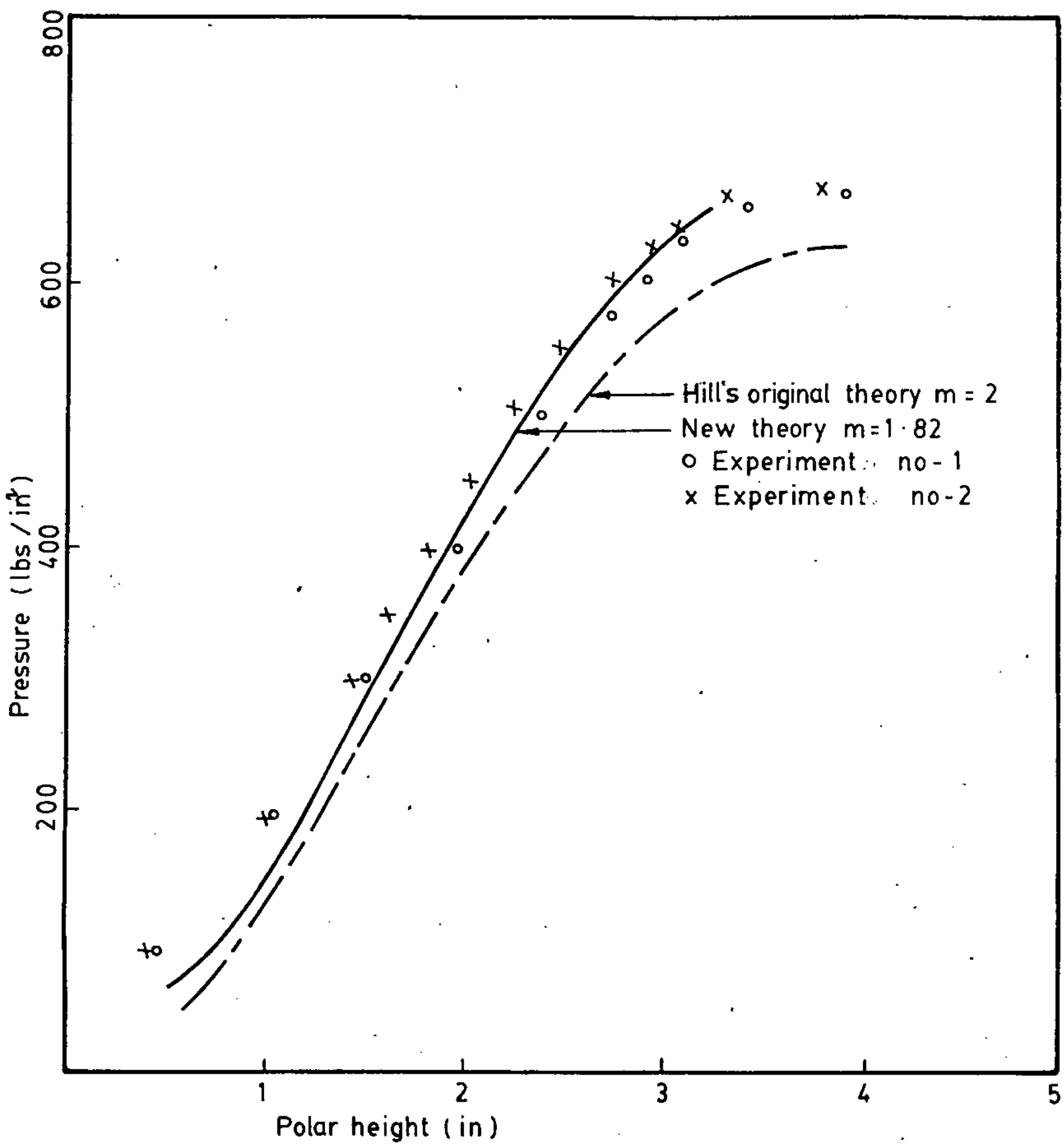

PRESSURE VS POLAR HEIGHT–SOFT BRASS
Comparison of experimental results with theoretical results
FIG·4·1·16

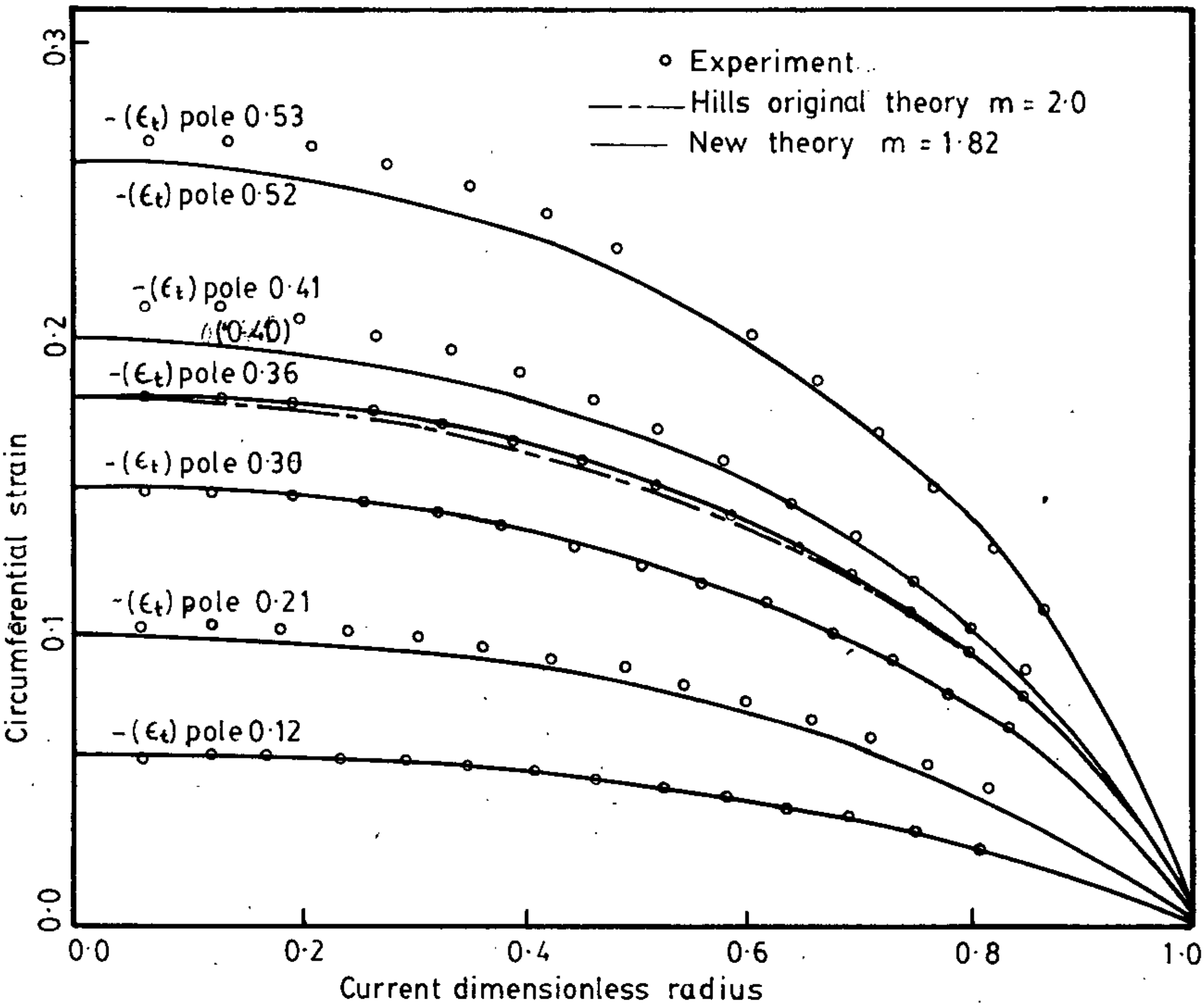

Theoretical and experimental circumferential strain distribution for soft 70/30 brass

FIG· 4·1·17

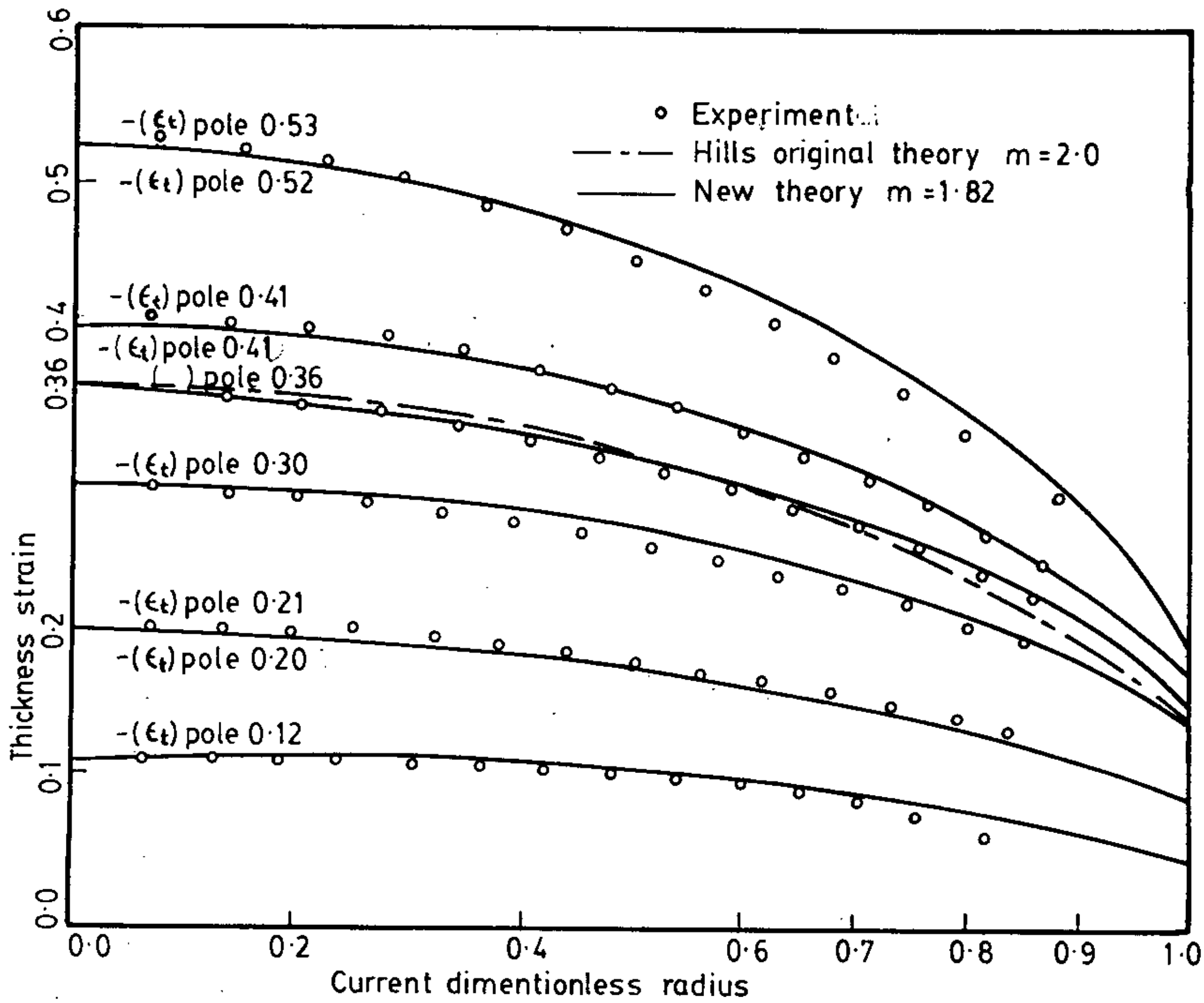

Theoretical and experimental thickness strain distribution for soft 70/30 brass
FIG·4·1·18

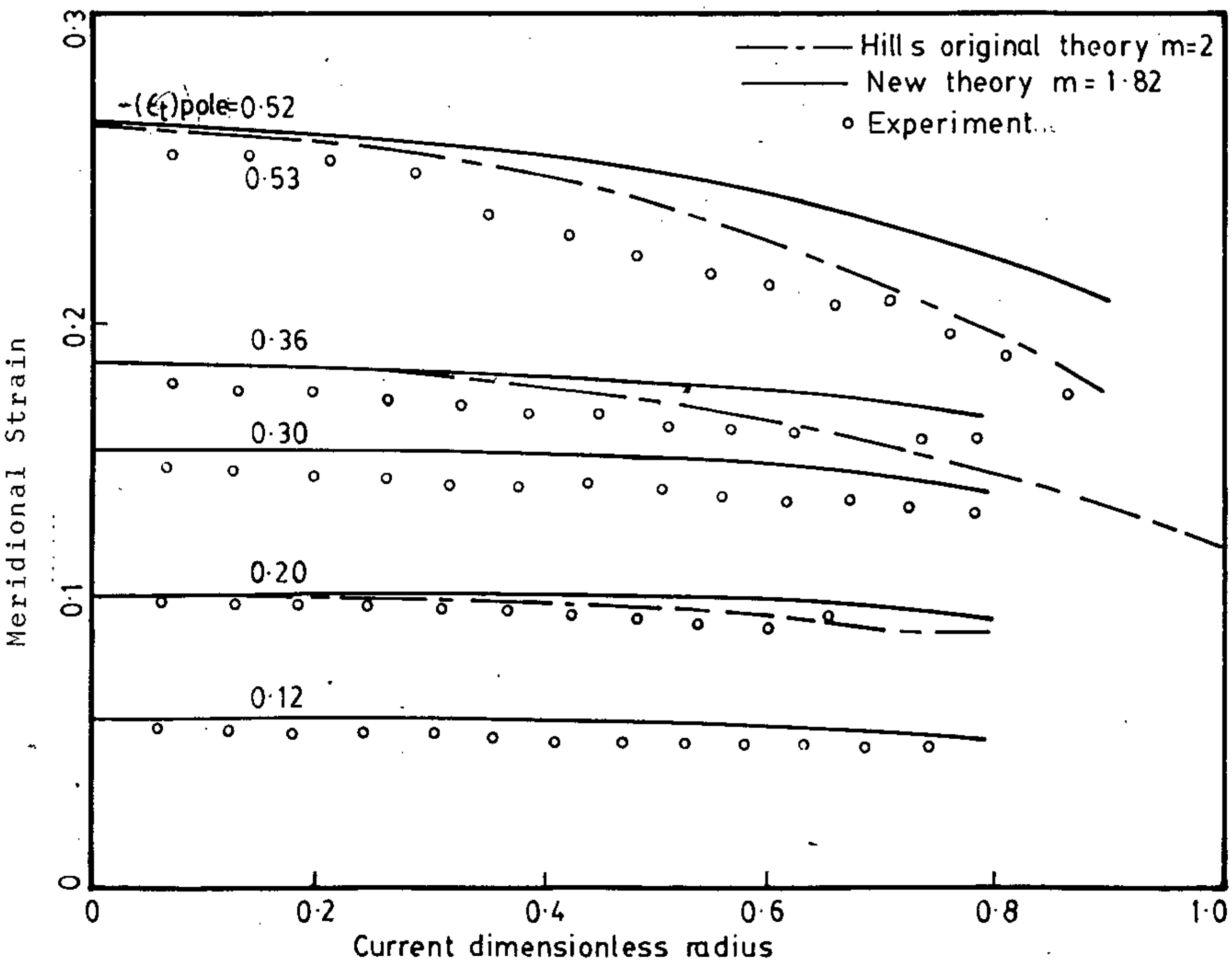

Theo. and Exp. Meridional strain distribution for soft 70/30 brass
FIG·4·1·19

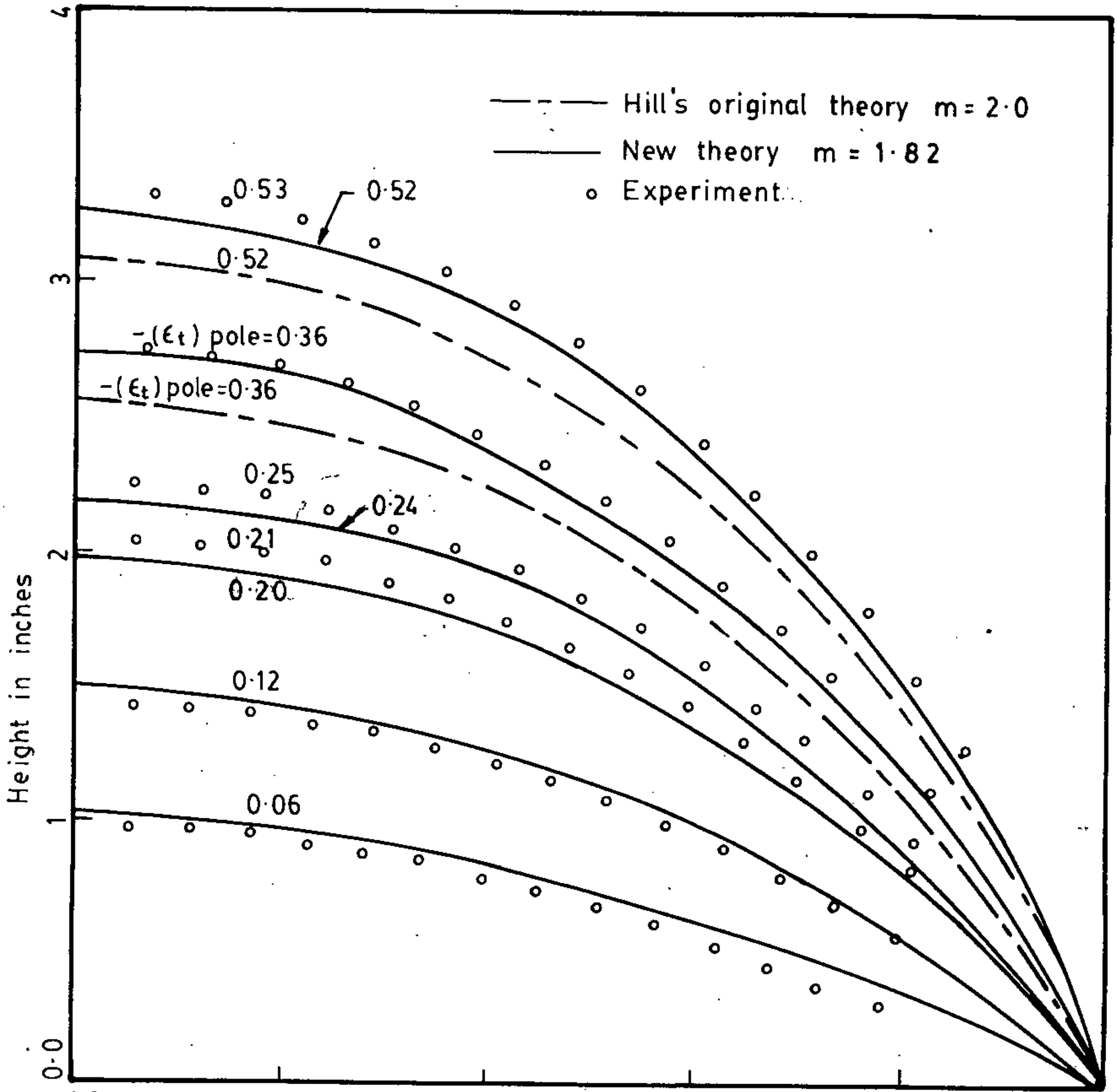

Height distribution soft brass

Theoretical and experimental height distribution for soft 70/30 brass

FIG·4·1·20

REFERENCES

1. Hill, R.
   'A theory of the plastic bulging of a metal diaphragm by lateral pressure'.
   Proc. Royal Soc. Ser. 7, Vol. 41, No.522, P. 1133 (1950).

2. Woo, D.M.
   'The analysis of axisymmetric forming of sheet metal and the hydrostatic bulging process'.
   Int. J. of Mech. Sci., Vol. 6, p. 303-319, (1964).

3. Chakrabarty, J. and Alexander, J.M.
   'Hydrostatic bulging of circular diaphragm'
   J. of Strain Analysis (inst. of Mech. Engrs.) Vol.5, No. 3, p. 155-161 (1970).

4. Bramley, A.N. and Mellor, P.B.
   'Plastic flow in stabilized sheet steel'.
   Int. J. of Mech. Sci. Vol. 8, p.101- 114, (1966).

5. Bramley, A.N. and Mellor, P.B.
   'Plastic anisotropy of titanium and zinc sheet - I - macroscopic approach'.
   Int. J. of Mech. Sci., Vol.10, p.211 - 219, (1968).

6. Wang, N.M. and Shammamy, M.R.
   'On the plastic bulging of a circular diaphragm by hydrostatic pressure'.
   J. of Mech. and Phys. of Solids, Vol.17, p.43-61, (1969).

7. Pearce, R.
   'Some aspects of anisotropic plasticity in sheet metal'.
   Int. J. Mech. Sci., Vol. 10, p. 995-1005, (1968).

8. Woodthorpe, J. and Pearce, R.
'The anomalous behaviour of aluminium sheet under balanced biaxial tension'.
Int. J. of Mech. Sci., Vol. 12, p. 341-347, (1970).

9. Yamada, Y. and Yokouchi, Y.
'Analysis of the hydraulic bulge test by the incremental theory of plasticity'. (in Japanese)
Seisan Kenkyu, Vol. 19, No. 12, p. 366, (1967).
Inst. Ind. Sci., Univ. of Tokyo.

10. Ilahi, M.F.
'Plastic Deformation of circular metal diaphragms'
Ph.D thesis, Univ. of Bradford (1977).

11. Parmar, A. and Mellor, P.B.
'Plastic expansion of a circular hole in sheet metal subjected to biaxial tensile stress'.
Int. J. of Mech. Sci., Vol. 20, p. 707-720 (1978).

12. Hill, R.
'Theoretical plasticity of textured aggregates'
Math. Camb. Phil. Soc. 85, (1979), p.179-191.

13. Hill, R and Storakers, B.
'Plasticity and Creep of Pressurized Membranes: A New Look at the Small-deflection theory".
J. Mech. and Phys. of Solids, Vol. 28, p.27-48, (1980).

14. Ilahi, M.F., Parmar, A. and Mellor, P.B.
'Hydrostatic bulging of a circular aluminium diaphragm'
Int. J. of Mech. Sci., Vol. 23, p.221-227, (1981).

15. Chater, E. and Neale, K.W.
'Finite plastic deformation of a circular membrane under hydrostatic pressure-I (Rate independent behaviour)'
Int. J. of Mech. Sci.,Vol.25,No.4, p.219-233 (1983).

16. Chater, E. and Neale, K.W.
'Finite plastic deformation of a circular membrane
under hydrostatic pressure-II (strain-rate effects)
Int. J. of Mech. Sci, Vol. 25, No.4, p.235-244 (1983).

17. Hill, R.
'The mathematical theory of plasticity'
Oxford University Press, Chap. 12 (1950).

18. Kobayashi, S. and Kim, J.H.
'Proc. Symp. on Mechanics of sheet metal forming,
341 (D.P. Koistinen and N.M. Wang, Eds.)
Plenum Press, New York (1978).

APPENDIX-I
NUMERICAL PROCEDURE

(i) Initial conditions: Along the radius of the bulge, $r = 0$ to $r = Ra$, initial conditions are

$$\sigma_r = \sigma_\theta = \varepsilon_\theta = \varepsilon_t = 0, \; t = t_o \text{ and } p = 0 \qquad (15)$$

ii) Boundary conditions:

a) the pole is assumed to strain under balanced biaxial tension, hence the boundary conditions at the pole ($r_o = 0$) are

$$\sigma_r = \sigma_\theta \, , \; \varepsilon_\theta = - \varepsilon_t/2, \; \rho_1 = \rho_2 \text{ and } \theta = 0 \qquad (16)$$

b) the circumferential strain, ε_θ is assumed to be zero at the edge.

$\varepsilon_\theta \simeq 0$ at $r = Ra$, for all stages of deformation

The procedure of solution is as follows:

At the pole,

i) A value of $(\varepsilon_t)_{i,j} = \Delta\varepsilon_t (= 0.02)$ at the pole ($i = 1$, $j = 1$, $r = 0$) is assumed.

ii) For this polar thickness strain the pressure is increased from 0 to an assumed value P_j. Since, at the pole

$\varepsilon_{\theta 1,j} = (-\varepsilon_t)_{1,j}/2$, hence $(\varepsilon_\theta)_{1,j}$, and $(\Delta\varepsilon_\theta)_{1,j}$.

$(\Delta\varepsilon_r)_{1,j}$ is found from equation $(d\varepsilon_\theta + d\varepsilon_r + d\varepsilon_t = 0)$

$(\Delta\bar{\varepsilon})_{1,j}$ from equation (7), hence $(\bar{\varepsilon})_{1,j}$. $(\bar{\sigma})_{1,j}$ from equation (8). $(\sigma_\theta)_{1,j}$ and $(\sigma_r)_{1,j}$ is computed from equations $(\sigma_\theta)_{1,j} = (\sigma_r)_{1,j} \overset{(\sigma_\theta+\sigma_r)}{\Lambda} = \left[(\bar{\sigma}/2)\{-(1+R)\,\Delta\varepsilon_t/\Delta\varepsilon\}^{1/m-1}\right]$, and $(t)_{1,j}$ from eqn. (a). Since σ_θ and σ_r are known, $(\rho_1)_{1,j} = (\rho_2)_{1,j}$ from equation $\rho_2 = 2\,\sigma_r t/P$.

Now all the computations are completed at the pole.

For the element next to the ple (i = 2) of initial radius $(r_o)_{i+1}$, the values $(t)_{i+1,j}$, $(\rho_1)_{i+1,j}$ and $(\rho_2)_{i+1,j}$ are assumed to be the same as that at the pole (i = 1), Then $\theta_{i+1,j}$ is found from equation (14), $\theta_{i+1,j}$ is now known next to compute current radius $r_{i+1,j} (= [\rho_2 + t/2]_{i+1,j} \sin\theta_{i+1,j})$. From the known values of current radius, $(\varepsilon_\theta)_{i+1,j} (= \ln[r_{i+1,j}/(r_o)_{i+1}])$, and $(\varepsilon_t)_{i+1,j}$ from $(= \ln[(t)_{i+1,j}/(t_o)])$, are found out then the finite strain increments are

$$
\begin{aligned}
(\Delta\varepsilon_\theta)_{i+1,j} &= (\varepsilon_\theta)_{i+1,j} - (\varepsilon_\theta)_{i+1,j-1} \\
\text{and } (\Delta\varepsilon_t)_{i+1,j} &= (\varepsilon_t)_{i+1,j} - (\varepsilon_t)_{i+1,j-1}
\end{aligned} \tag{17}
$$

$(\Delta\bar{\varepsilon})_{1+1,j}$, (finite generalized strain increment) is then found from equation (7) and hence generalized strain, $(\bar{\varepsilon})_{i+1,j}$

$$(\bar{\varepsilon})_{i+1,j} = \Sigma\,\Delta\bar{\varepsilon} = (\bar{\varepsilon})_{i+1,j-1} + (\Delta\bar{\varepsilon})_{i+1,j} \tag{18}$$

$(\bar{\sigma})_{i+1,j}$ is found from equation (8) and the stresses $(\sigma_r)_{i+1,j}$ and $(\sigma_\theta)_{i+1,j}$ are determined from combination of equation (12) and (13). For radial equilibrium, the equation (1) is then integrated numerically following the trapezoidal rule, gives a new value of $(t\sigma_r)'_{i+1,j}$ as

$$(t\sigma_r)'_{i+1,j} = (t\sigma_r)_{i,j} + \tfrac{1}{2}\{\left[\frac{t(\sigma_\theta-\sigma_r)}{r}\right]_{i,j}$$

$$+\left[\frac{t(\sigma_\theta-\sigma_r)}{r}\right]_{i+1,j}\}\left[(r)_{i+1,j}-(r)_{i,j}\right] \quad (19)$$

New values of $(\rho_2)_{i+1,j}$ and $(\rho_1)_{i+1,j}$ are found from equation (2) and (3) as

$$(\rho_2)_{i+1,j} = \frac{2(t\sigma_r)'_{i+1,j}}{(P)_j} \quad (20)$$

Again $(t\sigma_\theta)'_{i+1,j}$ is expressed as

$$(t\sigma_\theta)'_{i+1,j} = (t\sigma_r)'_{i+1,j} + [t(\sigma_\theta-\sigma_r)]_{i+1,j}$$

then, $$(\rho_1)_{i+1,j} = \frac{2\left[(t\sigma_r)'_{i+1,j}\right]^2}{(P)_j\left[2(t\sigma_r)'_{i+1,j} - (t\sigma_\theta)'_{i+1,j}\right]} \quad (21)$$

The new value of $(t)'_{i+1,j}$ is found by substituting $(t\sigma_r)'_{i+1,j}$ and $(t\sigma_\theta)'_{i+1,j}$ into the following equation which is based on equation (11).

$$(\Delta\varepsilon_t)'_{i+1,j} = -\left[\frac{(t\bar{\sigma}_\theta)'_{i+1,j} + (t\sigma_r)'_{i+1,j}}{(t\sigma)_{i+1,j}}\right]^{m-1}\frac{(\Delta\bar{\varepsilon})_{i+1,j}}{(1+R)} \quad (22)$$

From equation (17), with new value of $(\Delta\varepsilon_t)'_{i+1,j}$, $(\varepsilon_t)'_{i+1,j}$ is found and hence $(t)'_{i+1,j}$. The next cycle of computation is carried out with these new values of $(\rho_1)_{i+1,j}$, $(\rho_2)_{i+1,j}$ and

$(t)_{i+1,j}$ and continued until the radial equilibrium condition is satisfied i.e $(t\ \sigma_r)'_{i+1,j}$ is equal to $[(t)_{i+1,j} \cdot (\sigma_r)_{i+1,j}]$.

Above iterative procedure is satisfactory only upto the point next to the pole, when incremental strain, $(\Delta\varepsilon_t)_{pole} \leqslant 0.05$ is considered. The solution becomes divergent beyond the point next to the pole due to an inappropriate assumptions of the initial values of $(\rho_1)_{3,j}$ and $(\rho_2)_{3,j}$, equal to the values of $(\rho_1)_{2,j}$ and $(\rho_2)_{2,j}$ respectively which leads $(\varepsilon_\theta)_{3,j} > (\varepsilon_\theta)_{2,j}$. In order to overcome this situation, first approximation of $(\varepsilon_\theta)_{i+1,j}$ is estimated directly using the equation for compatability of strain, written in a finite difference form, the equation (e) as

$$(\varepsilon_\theta)_{i+1,j} = (\varepsilon_\theta)_{i,j} + \left[\frac{\exp(\varepsilon_r - \varepsilon_\theta)_{i,j} \cos\theta_{i,j} - 1}{(r_o)_i}\right] \times [(r_o)_{i+1} - (r_o)_i]$$

It is pointed out that the above equation is only used for the initial approximation of $(\varepsilon_\theta)_{i+1,j}$ at each point on the radius characteristics $(r_o)_{i,j} \geqslant (r_o)_{3,j}$.

The above procedure for stage j is continued along the radius characteristics upto the fixed edge of the bulge radius Ra. the solution is considered correct when $(\varepsilon_\theta) \simeq 0$ at the fixed edge at radius Ra.

This condition is achieved only when the pressure corresponding the polar strain is correctly assumed for that particular stage j. Correct pressure is obtained by trial and error. A method of successive approximation using linear inter-polation or extrapolation has been used for this present work which in details are given below.

First, with the assumed pressure $(P)_j$ all the deformation parameters are computed, if the boundary conditions are not satisfied, then a new pressure is assumed with the formula

$$(P)_j = (P)_j + \Delta P \qquad (23)$$

where ΔP is a small increment in pressure, when two steps of trial has been completed the next approximation is made as follows.

Let us suppose that in the first step pressure is P_j' and circumferential strain, ε_θ at the edge is ε_θ' and similarly for the second step, P_j'' and ε_θ''. Since we are interpolating or extrapolating linearly

$$Y = mx + c$$

$\therefore$ we have

$$P'' = m\,\varepsilon_\theta'' + c \qquad \text{(i)}$$

$$P' = m\,\varepsilon_\theta' + c \qquad \text{(ii)}$$

Solving equation (i) and (ii) for c

$$c = \frac{P''\varepsilon_\theta' - P'\varepsilon_\theta''}{\varepsilon_\theta' - \varepsilon_\theta''}$$

$$\therefore \quad P''' = \frac{P''\varepsilon_\theta' - P'\varepsilon_\theta''}{\varepsilon_\theta' - \varepsilon_\theta''} \qquad (24)$$

To reduce the time required for calculation, the approximation for pressure for every stage can be performed with the above two equations (23) and (24).

When a satisfactory result for a stage is found the height distribution is determined from the equation

$$\frac{dy}{dr_o} = - \sin\theta \, e^{\varepsilon_r} \tag{25}$$

where y is the height of the bulge at angle θ measured from the pole. The equation (25) is integrated using a finite difference form, starting with the condition at the fixed edge r = Ra, y = 0.

APPENDIX II
ALGORITHM

1. Insert the values for R, M, n, k, t_o, increment of ε_t , small increment of pressure and a approximate value of pressure for the stage (2).

2. Divide $r_o = 0.0$ to r_o= Ra with desired no. of points, (For this present analysis 47 points were considered, at the pole $r_o = 0.0$ and first radius to the point next to the pole is 0.5 and then with increment of 0.1).

3. $\bar{\varepsilon}$, ε_t, ε_θ and $\varepsilon_r = 0.0$ for the stage j = 1 and i = 1, KP.

4. $r_{1,j} = 0.0$ and $\theta_{1,j} = 0.0$, for all the J s.

5. J = 2 to IP (start with first value of J)

6. At the pole: Calculate, $\varepsilon_{t(1,j)}$, $d\varepsilon_{t(1,j)}$, $\varepsilon_{\theta(1,j)}$ $d\varepsilon_{\theta(1,j)}$, $d\varepsilon_{r(1,j)}$, $\varepsilon_{r(1,j)}$ $d\bar{\varepsilon}$, $\bar{\varepsilon}$, $\bar{\sigma}$, σ_r, σ_θ , ρ_1, ρ_2 and t.

7. For the point next to the pole:

   Initialize, $(\rho_1)_{2,j} = (\rho_1)_{1,j}$, $(\rho_2)_{2,j} = (\rho_2)_{1,j}$, $(t)_{2,j} = t_{(1,j)}$.

8. Compute, θ , r, ε_θ, $d\varepsilon_\theta$, ε_t, $d\varepsilon_t$, $d\varepsilon_r$, ε_r, $d\bar{\varepsilon}$, $\bar{\varepsilon}$, $\bar{\sigma}$, σ_r, σ_θ and $(t\sigma_r)'$

9. Check $[(t^*\sigma_r)/(t\sigma_r)]' \leq 1 \pm 0.00003$,

   if (yes) then to 13

   if (no) then to 10

10. Compute $(t\sigma_\theta)'$, ρ_2', ρ_1', $\Delta\varepsilon_t'$ and t'

11. Initialize ρ_2, ρ_1 and t with ρ_2', ρ_1' and t'

12. Repeat 8-11 until, (9) is satisfied.

13. For the points beyond the point next to the pole:

    I = 2, (KP-1), start with first value of I.

    Initialize $\rho_{1(I+1,j)} = \rho_{1(i,j)}$

    $\rho_{2(i+1,j)} = \rho_{2(i,j)}$

    $t_{(i+1,j)} = t_{i(i,j)}$

14. Compute ε_θ from strain compatability eqn. and current radius, r.

15. Compute $\theta_{(i+1,j)}$, $\varepsilon t_{(i+1,j)}$, $d\,\varepsilon_{t(i+1,j)}$, $d\varepsilon_\theta(i+1,j)$, $d\,\varepsilon_{r(i+1,j)}$, $\bar{\varepsilon}_{(i+1,j)}$, $\bar{\sigma}_{(i+1,j)}$, $\sigma_{r(i+1,j)}$, $\sigma_{\theta(i+1,j)}$ and $(t\sigma_r)'_{(i+1,j)}$

16. Check $[(t^*\sigma_r)/(t\sigma_r)']_{(i+1,j} \leqslant 1 \pm 0.00003$

    If (yes) then to 13 (for the next value of i)

    and if (no) then to 17.

17. Compute, $(t\sigma_\theta)'_{(i+1,j)}$, $\rho'_{2(i+1,j)}$, $\rho'_{1(i,1,j)}$, $t'_{(i+1,j)}$

18. Initialize $\rho_{2(i+1,j)}$, $\rho_{1(i+1,j)}$ and $t_{(i+1,j)}$ with new values.

19. Repeat 15-18 till 16 is satisfied.

20. Continue 13-19 for all values of i.

21. Check $(\varepsilon_\theta)_{edge} \leqslant 0.0003$ and $\geqslant -0.0003$

    If (yes) then to 25

    If (no) then to 22

22. Find a new value of pressure either from $P = P + \Delta P$ or from linear interpolation and extrapolation formulae.

23. Repeat 6-21, until the condition 21 is satisfied.

24. Compute height for each point, $h_{(i,j)}$.

25. Write, i, j, θ, r_o, r, $\bar{\sigma}, \bar{\varepsilon}$, t, ε_r, ε_θ, ε_t, σ_r, σ_θ $(t*\sigma_r)/(t\sigma_r)$ and h.

    Check $P_{(j)} < P_{(j-1)}$,

    If (yes) then to 27

    If (no) then to 26

26. DO 5-23 for the next value of J, upto the last value of j.

27. STOP

APPENDIX-III

FLOW CHART

START

Input :
R, m, n, k, t_o, increment of ε_t, small increment of pressure, and approximate value of pressure, p.

Choose the number of points, with desired interval of radius along the original radius characteristics. Such that $r_o = 0$ at pole $r_o = Ra$ at the edge.

For I=1, KP J = 1
$\bar{\varepsilon} = \varepsilon_t = \varepsilon_\theta = \varepsilon_r = 0.0$
I, continued

(11)

For J = 2, IP
$r(1,j) = 0.0, \theta(1,j) = 0.0$
J, continued

(10)

J = 2, IP (Start with first value of J) and LP = 1

At the pole: compute
ε_t, $d\varepsilon_t$, ε_θ, $d\varepsilon_\theta$, $d\varepsilon_r$, ε_r $\bar{\sigma}$
$d\bar{\varepsilon}$, $\bar{\varepsilon}$, σ_r, σ_θ, t, ρ_1 and ρ_2.

For the point next to the pole
$(\rho_1)(2,j) = (\rho_1)_{i,j}$, $(\rho_2)_{2,j} = (\rho_1)_{i,j}$
$t_{2,j} = t_{1,j}$
L = 1

(1)

(12)

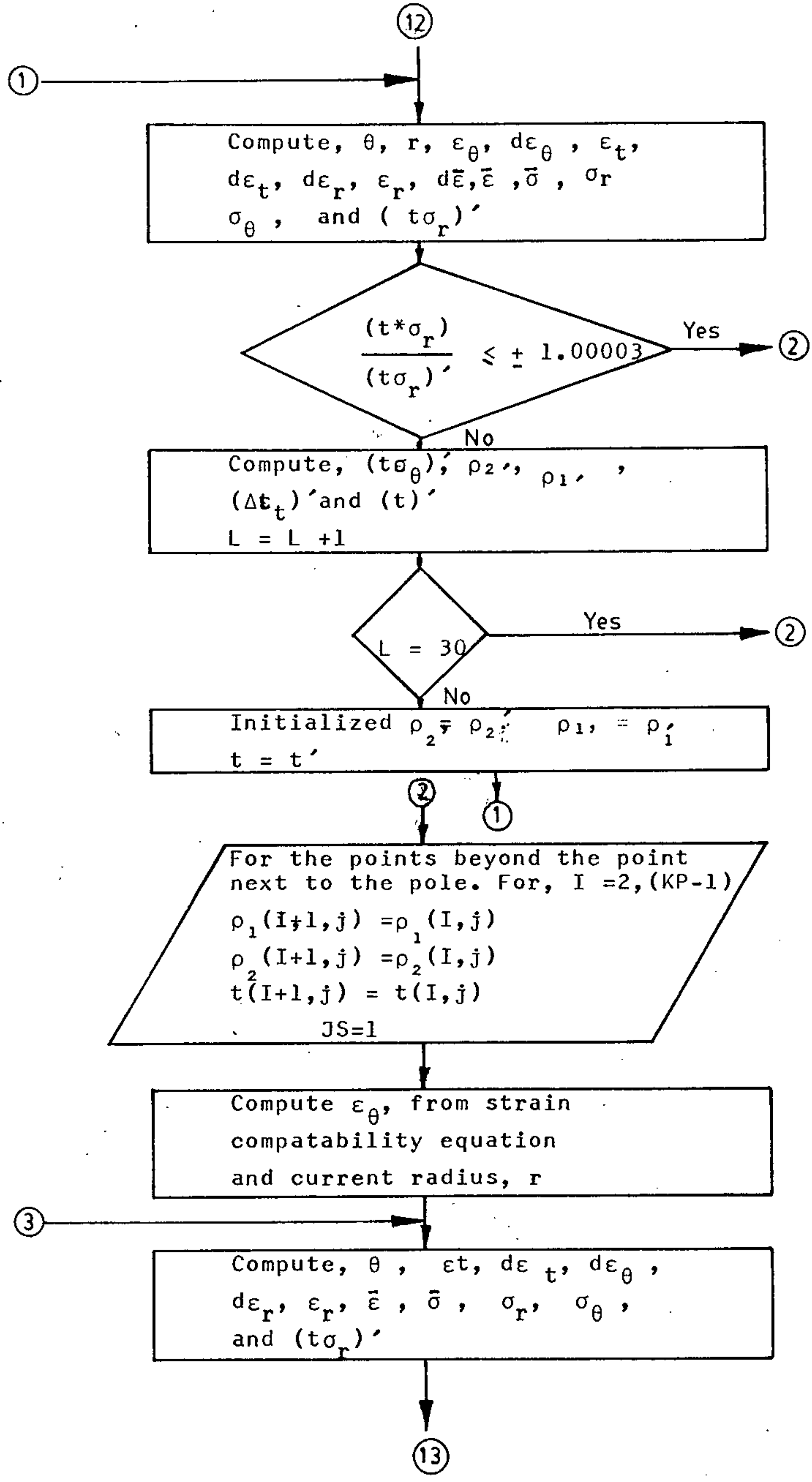
12
1
Compute, θ, r, εθ, dεθ , εt,
dεt, dεr, εr, dε̄, ε̄ , σ̄ , σr
σθ , and (tσr)′
(t*σr) / (tσr)′ ≤ ± 1.00003
Yes
2
No
Compute, (tσθ)′, ρ2′, ρ1′ ,
(Δtt)′and (t)′
L = L +1
L = 30
Yes
2
No
Initialized ρ2 = ρ2′ ρ1, = ρ1′
t = t′
2
1
For the points beyond the point
next to the pole. For, I =2,(KP-1)
ρ1(I+1,j) =ρ1(I,j)
ρ2(I+1,j) =ρ2(I,j)
t(I+1,j) = t(I,j)
JS=1
Compute εθ, from strain
compatability equation
and current radius, r
3
Compute, θ , εt, dε t, dεθ ,
dεr, εr, ε̄ , σ̄ , σr, σθ ,
and (tσr)′
13

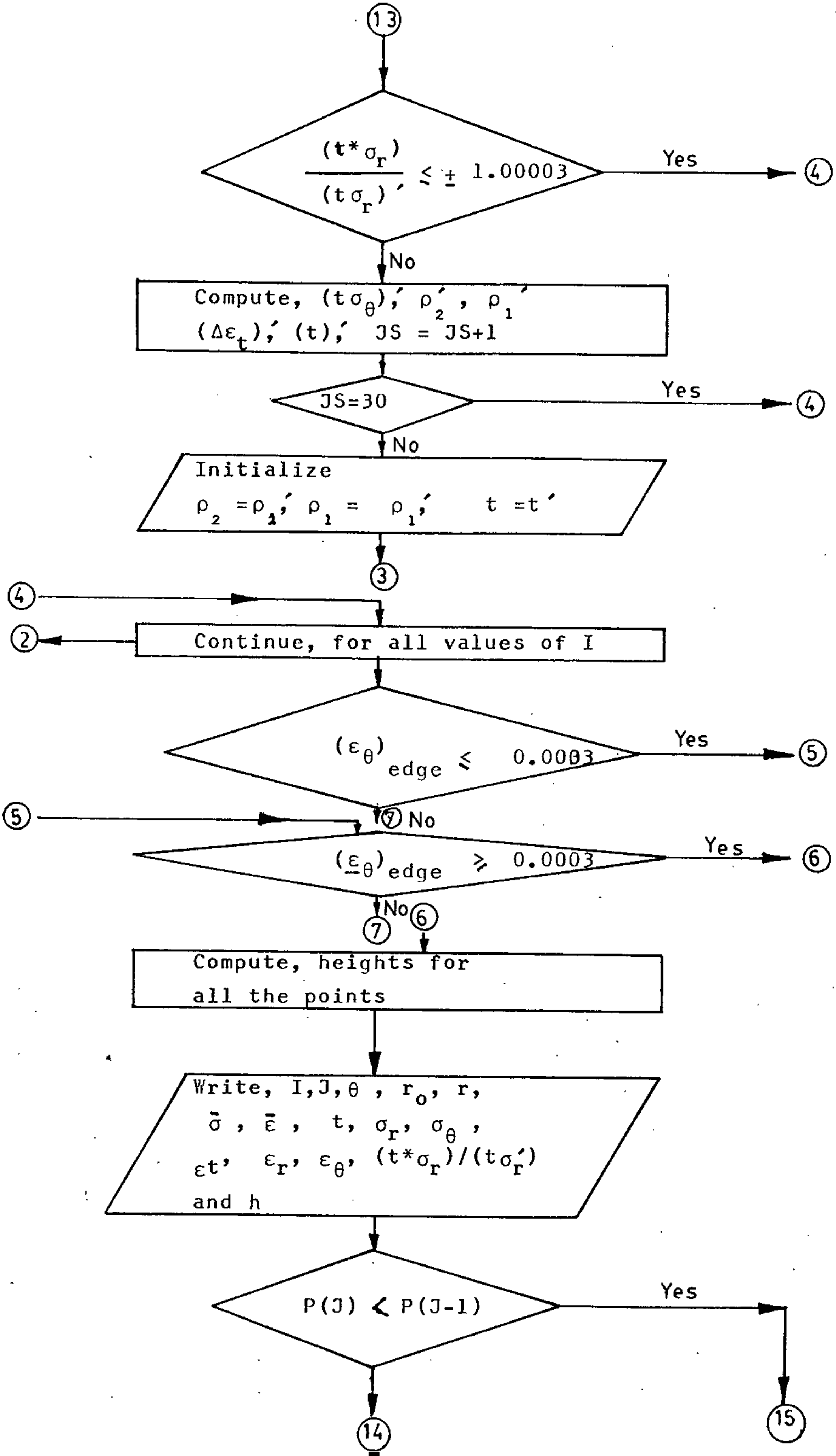
13
$\frac{(t^*\sigma_r)}{(t\sigma_r)'} \leq \pm 1.00003$
Yes
4
No
Compute, $(t\sigma_\theta)'$, ρ_2', ρ_1'
$(\Delta\varepsilon_t)'$, $(t)'$, JS = JS+1
JS=30
Yes
4
No
Initialize
$\rho_2 = \rho_2'$, $\rho_1 = \rho_1'$, $t = t'$
3
4
2
Continue, for all values of I
$(\varepsilon_\theta)_{edge} \leq 0.0003$
Yes
5
5
7
No
$(\varepsilon_\theta)_{edge} \geq 0.0003$
Yes
6
No
7
6
Compute, heights for
all the points
Write, I, J, θ, r_o, r,
$\bar{\sigma}$, $\bar{\varepsilon}$, t, σ_r, σ_θ,
εt, ε_r, ε_θ, $(t^*\sigma_r)/(t\sigma_r')$
and h
P(J) < P(J-1)
Yes
14
15

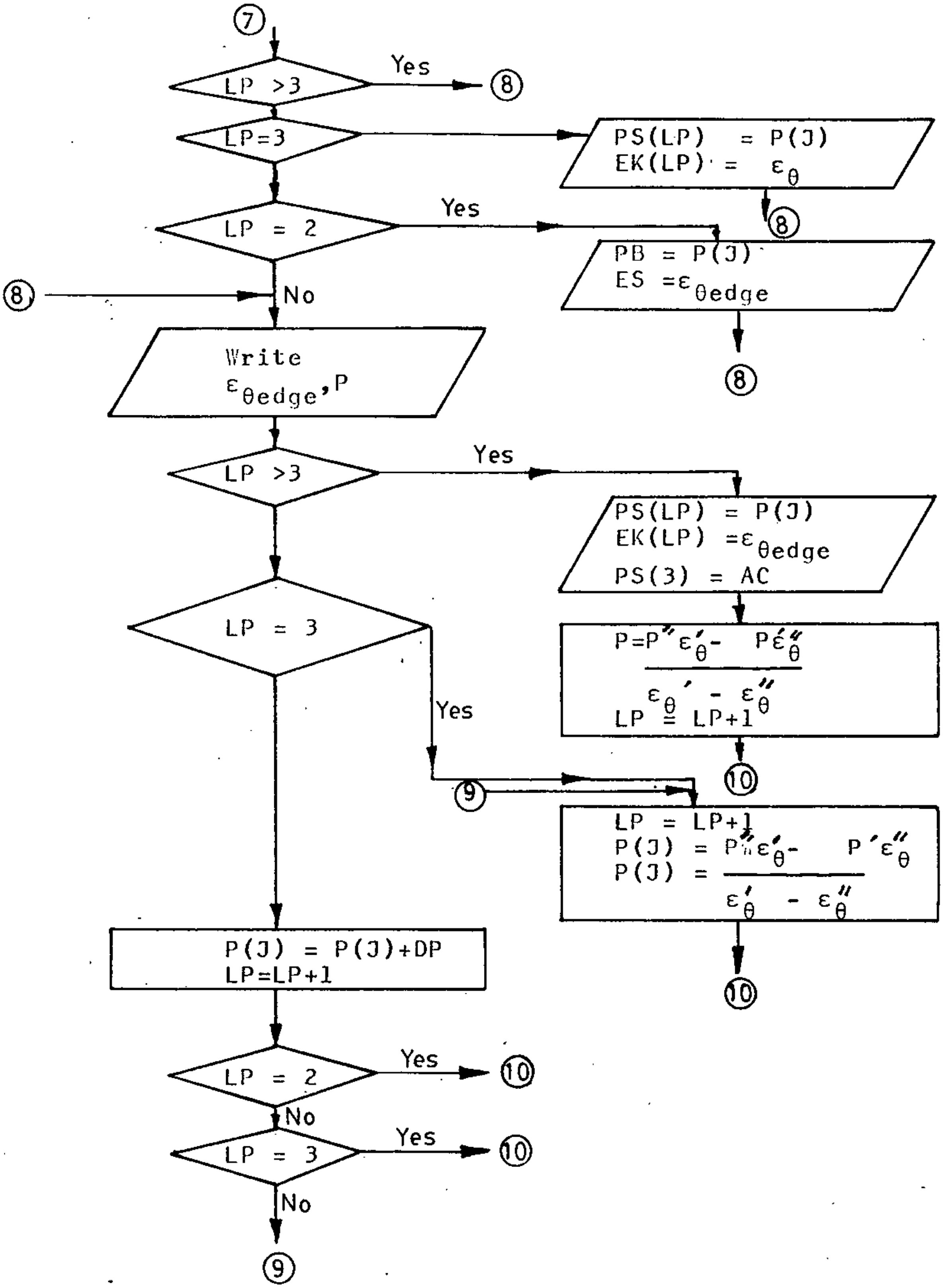

7
LP >3
Yes
8
LP=3
PS(LP) = P(J)
EK(LP) = ε_θ
8
LP = 2
Yes
PB = P(J)
ES = ε_θedge
8
No
8
Write
ε_θedge, P
LP >3
Yes
PS(LP) = P(J)
EK(LP) = ε_θedge
PS(3) = AC
LP = 3
P=P″ε′_θ - Pε″_θ / ε′_θ - ε″_θ
LP = LP+1
Yes
10
9
LP = LP+1
P(J) = P″ε′_θ - P′ε″_θ
P(J) = / ε′_θ - ε″_θ
10
P(J) = P(J)+DP
LP=LP+1
LP = 2
Yes
10
No
LP = 3
Yes
10
No
9

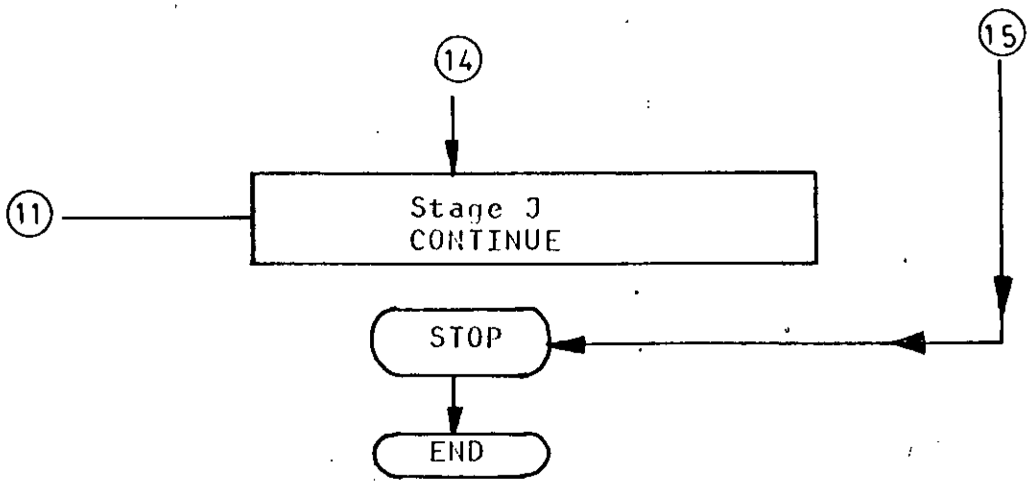
14
15
11
Stage J
CONTINUE
STOP
END

APPENDIX-IV

COMPUTER PROGRAMME

```
// JOB NTOBSTAR MIDE
// OPTION LINK,LIST,LOG
// EXEC FFORTRAN
C       THIS PROGRAM HAS BEEN SUBMITTED TO THE DEPTT.OF MECHANICAL ENGG.
C       ,BUET. FOR THE FULFILMENT OF THESIS WORK BY TAPAN KUMAR PAUL UND
C       ER SUPERVISSION OF DR. M.H.ILAHI, IN PARTIAL FULFILMENT FOR THE
C       DEGREE OF M.SC.ENGG.(MECHANICAL)
C
C
C       THIS THEORITICAL ANALYSIS IS APPLIED TO THE BULGING OF SOFT 70/30
C        BRASS .IS BASED ON THE  NEW ANISOTROPIC  YIELD CRITERION PROPOSED
C        PROFESSOR HILL IN MATHEMATICAL  CAMBRIDGE PHILOSOPHICAL SOCIETY
C       85 , 179, (1979).
        REAL M,N,K
        DIMENSION RD(50), P(50),ET(50,45),DET(50,45),EO(50,45),DEO(50,45),
       *DER(50,45),DEG(50,45),EE(50,45),SIGE(50,45),SIGR(50,45),SIGO(50,45
       *) ,T(50,45),RC1(50,45),RC2(50,45),TH(50,45),RC(50,45),ER(50,45),
       *TSIG(50,45),TSIF(50,45),EOIP(50,45),RLEF(50,45),DETP(50,45),PET
       *(50,45),PT(50,45),AB(50),PS(50),EK(50),PRES(50),Z(50,45),SOFT(50)
       *,CCF(50)
C       INITIAL CONDITIONS
C
        DP=0.5
        DT=-0.02
        DO 440  I=1,47
        EE(I,1)=0.0
        ET(I,1)=0.0
        EO(I,1)=0.0
        ER(I,1)=0.0
  440   CONTINUE
        R=0.860
        M=1.820
        TO=0.0376
        READ(1,3)K,N
  3     FORMAT(2F10.3)
        READ(1,945)(PRES(I),I=2,30)
  945   FORMAT(F14.7)
        RD(1)=0.0
        RD(2)=0.5
```

```
      DC 57 I=2,46
      RD(I+1)=RD(I)+J.1
      IC=I+1
      WRITE(3,233) IC, RD(IC)
 233  FORMAT(/,5X,I3,10X,F14.7)
 57   CONTINUE
C     P(1)=90.00
      DO 37 J=2,30
      LP=1
      IF( J.GT.30) GO TC 111
      P(J)=PRES(J)
      GC TC 9
C
 111  P(J)=P(J-1)
C
C     AT THE POLE,THE POINT 1.LO.1
C
 9    ET(1,J)=ET(1,J-1)+DI
      DET(1,J)=ET(1,J)-ET(1,J-1)
      EC(1,J)=-ET(1,J)/2.
      DEC(1,J)=EO(1,J)-EO(1,J-1)
      DER(1,J)=-DET(1,J)-DEC(1,J)
      ER(1,J)=DER(1,J)+ER(1,J-1)
      C1=((2*(1+R))**(1./M))/2.
      C2=((ABS(DEO(1,J)-DER(1,J)))**(M/
     .(M-1)))/(1+2*R)**(1./(M-1))
      C3=(ABS(DEO(1,J)+DER(1,J)))**(M/(M-1))
      DEG(1,J)=C1*((C2+C3)**((M-1)/M))
      EB(1,J)=DEG(1,J)+EB(1,J-1)
      IF(EB(1,J).LE.0.111) GO TO 701
      SIGB(1,J)=K*(EB(1,J)**N)
```

```
      GO TO 702
  701 SIGB(1,J)=(115330.00)*((0.042+EB(1,J)))**0.624
C
  702 V=-(1+R)*(DET(1,J)/DEG(1,J))
      SIGR(1,J)=(SIG3(1,J)/2.)*(V**(1./(M-1)))
      SIGC(1,J)=SIGR(1,J)
      T(1,J)=TO*EXP(ET(1,J))
      RO2(1,J)=(2*(SIGR(1,J)*T(1,J)))/P(J)
      RO1(1,J)=RO2(1,J)
C
C
C
C
C     OPERATION AT THE POLE IS  COMPLETED
C
C
C     OPERATION  FOR THE POINT NEXT TO  THE POLE STARTS.
C
      RC(1,J)=0.0
      TH(1,J)=0.0
      RO1(2,J)=RO1(1,J)
      RO2(2,J)=RO2(1,J)
      T(2,J)=T(1,J)
      L=1
C
C
   27 E1=(RO1(1,J)+RO1(2,J))/2.+(T(1,J)+T(2,J))/4.0
      E2=(RO2(1,J)+RO2(2,J))/2.0+(T(1,J)+T(2,J))/4.0
      E3=(T(1,J)+T(2,J))/2.0
      E4=(RD(2)**2-RD(1)**2)*TL
      TH(2,J)=ARCOS(COS(TH(1,J))-((E4)/(2*E1*E2*E3)))
      RC(2,J)=(RO2(2,J)+T(2,J)/2.0)*SIN(TH(2,J))
      EO(2,J)=ALOG(RC(2,J)/RD(2))
      DEO(2,J)=EO(2,J)-EO(2,J-1)
      ET(2,J)=ALOG(T(2,J)/TO)
      DET(2,J)=ET(2,J)-ET(2,J-1)
      DER(2,J)=-DET(2,J)-DEO(2,J)
      ER(2,J)=DER(2,J)+ER(2,J-1)
      C1=((2*(1+R))**(1./M))/2.0
      C2=((ABS(DEO(2,J)-DER(2,J)))**(M/(M-1)))/(1+2*R)**(1./(M-1))
      C3=(ABS(DEO(2,J)+DER(2,J)))**(M/(M-1))
      DEG(2,J)=C1*((C2+C3)**((M-1)/M))
      EB(2,J)=DEG(2,J)+EB(2,J-1)
      IF(EB(2,J).LE.0.111) GO TO 703
      SIGB(2,J)=K*((EB(2,J))**N)
      GO TO 704
  703 SIGB(2,J)=(115330.00)*((0.042+EB(2,J)))**0.624
```

```
704   Q=-(1+R)*(DET(2,J)/DEG(2,J))
      H=((2*(1+R))/(1+2*R))*((DEG(2,J)+(DET(2,J)/2.0))/DEG(2,J))
      H1=((2*(1+R))/(1+2*R))*(ABS((DEG(2,J)+(DET(2,J)/2.0))/DEG(2,J)))
      IF(DEG(2,J).GT.DER(2,J)) GO TO 17
      IF(DEG(2,J).LT.DER(2,J)) GO TO 18
17    SIGO(2,J)=(SIG3(2,J)/2.0)*(Q**(1./(M-1))+H **(1./(M-1)))
      SIGR(2,J)=(SIG3(2,J)/2.0)*(Q**(1./(M-1))-H **(1./(M-1)))
      GO TO 19
18    SIGR(2,J)=(SIG3(2,J)/2.0)*(Q**(1./(M-1))+H1**(1./(M-1)))
      SIGO(2,J)=(SIG3(2,J)/2.0)*(Q**(1./(M-1))-H1**(1./(M-1)))
19    S=(T(2,J)*(SIGO(2,J)-SIGR(2,J)))/RO(2,J)
      TSIG(2,J)=(T(1,J)*SIGR(1,J))+(S/2.)*(RO(2,J)-RO(1,J))
      AB(2)=(T(2,J)*SIGR(2,J))/TSIG(2,J)
      IF(ABS(AB(2)-1.00000).LT.0.00003) GO TO 29
      TSIP(2,J)=TSIG(2,J)+T(2,J)*(SIGO(2,J)-SIGR(2,J))
      RO2P(2,J)=(2*(TSIG(2,J)))/P(J)
      RO1P(2,J)=(2*(TSIG(2,J))**2)/(P(J)*(2*TSIG(2,J)-TSIP(2,J)))
      FC=ABS((TSIP(2,J)+TSIG(2,J))/(T(2,J)*SIGO(2,J)))
      DETP(2,J)=-(FC**(M-1))*(DEG(2,J)/(1+R))
      ET(2,J)=DETP(2,J)+ET(2,J-1)
      PT(2,J)=TO*EXP(ET(2,J))
      T(2,J)=PT(2,J)
      RO1(2,J)=RO1P(2,J)
      RO2(2,J)=RO2P(2,J)
      L=L+1
      IF(L.EQ.31) GO TO 29
      GO TO 27
C
C     FOR THE POINTS BEYOND THE POINT NEXT TO THE POLE
C
29    DO 36 I=2,46
      RO1(I+1,J)=RO1(I,J)
      RO2(I+1,J)=RO2(I,J)
      T(I+1,J)=T(I,J)
```

```
      MS=1
      EE(I+1,J)=EO(I,J)+(((EXP(ER(I,J)-EO(I,J)))*COS(TH (I,J))-1.0)/
     .RD(I))*(RD(I+1)-RD(I))
      RC(I+1,J)=RD(I+1)*(EXP(EE(I+1,J)))
54    E1=(RO1(I,J)+RO1(I+1,J))/2.0+(T(I,J)+T(I+1,J))/4.0
      E2=(RO2(I,J)+RO2(I+1,J))/2.0+(T(I,J)+T(I+1,J))/4.0
      E3=(T(I,J)+T(I+1,J))/2.0
      E4=(RD(I+1)**2-RD(I)**2)*T0
      TH(I+1,J)=ARCOS(COS(TH(I,J))-((E4)/(2*E1*E2*E3)))
      DEO(I+1,J)=EO(I+1,J)-EO(I+1,J-1)
      ET(I+1,J)=ALOG(T(I+1,J)/T0)
      DET(I+1,J)=ET(I+1,J)-ET(I+1,J-1)
      DER(I+1,J)=-DET(I+1,J)-DEO(I+1,J)
      ER(I+1,J)=DER(I+1,J)+ER(I+1,J-1)
      C1=((2*(1+R))**(1./M))/2.0
      C2=((ABS(DEO(I+1,J)-DER(I+1,J)))**(M/(M-1)))/(1+2*R)**(1./(M-1))
      C3=(ABS(DEO(I+1,J)+DER(I+1,J)))**(M/(M-1))
      DEG(I+1,J)=C1*((C2+C3)**((M-1)/M))
      EB(I+1,J)=DEG(I+1,J)+EB(I+1,J-1)
      IF(EB(I+1,J).LE.0.111) GO TO 705
      SIGE(I+1,J)=K*((EE(I+1,J))**N)
      GO TO 708
705   SIGE(I+1,J)=(115330.00)*((0.042+EB(I+1,J)))**0.324
708   G=-(1+R)*(DET(I+1,J)/DEG(I+1,J))
      H=((2*(1+R))/(1+2*R))*((DEO(I+1,J)+(DET(I+1,J)/2.0))/DEG(I+1,J))
      H1=((2*(1+R))/(1+2*R))*(ABS((DEO(I+1,J)+(DET(I+1,J)/2.0))/DEG(I+
     .1,J)))
      IF(DEO(I+1,J).GT.DER(I+1,J)) GO TO 21
      IF(DEO(I+1,J).LT.DER(I+1,J)) GO TO 22
21    SIGO(I+1,J)=(SIGE(I+1,J)/2.0)*(Q**(1./(M-1))+H **(1./(M-1)))
      SIGR(I+1,J)=(SIGB(I+1,J)/2.0)*(Q**(1./(M-1))-H **(1./(M-1)))
      GO TO 20
22    SIGR(I+1,J)=(SIGE(I+1,J)/2.0)*(Q**(1./(M-1))+H1**(1./(M-1)))
      SIGO(I+1,J)=(SIGB(I+1,J)/2.0)*(Q**(1./(M-1))-H1**(1./(M-1)))
20    S=((T(I,J)*(SIGO(I,J)-SIGR(I,J)))/RC(I,J))+(T(I+1,J) *(SIGO(I+1
     .,J)-SIGR(I+1,J)))/RC(I+1,J)
      TSIG(I+1,J)=(T(I,J)*SIGR(I,J))+(S/2.0)*(RC(I+1,J)-RC(I,J))
      AB(I+1)=(T(I+1,J)*SIGR( I+1,J))/TSIG(I+1,J)
      IF(ABS(AB(I+1)-1.00000).LE.0.00005) GO TO 35
      TSIP(I+1,J)=TSIG(I+1,J)+T(I+1,J)*(SIGO(I+1,J)-SIGR(I+1,J))
      RO1P(I+1,J)=(2*(TSIG(I+1,J))**2)/(P(J)*(2*TSIG(I+1,J)-TSIP(I+1,
     .J)))
      RO2P(I+1,J)=(2*(TSIG(I+1,J)))/P(J)
      FC=ABS((TSIP(I+1,J)+TSIG(I+1,J))/(T(I+1,J)*SIGO(I+1,J)))
```

```
      DETP(I+1,J)=-(FC**(N-1))*(DEG(I+1,J)/(I+K))
      ET(I+1,J)=DETP(I+1,J)+ET(I+1,J-1)
      PT(I+1,J)=TC*(EXP(ET(I+1,J)))
      T(I+1,J)=PT(I+1,J)
      RC1(I+1,J)=RJ1P(I+1,J)
      RC2(I+1,J)=RJ2P(I+1,J)
      MS=MS+1
      IF(MS.EQ.C1) GO TO 36
      GO TO 54
 36   CONTINUE
C
C
C     ALL THE POINTS HAVE BEEN CALCULATED. ALL THE RESULTS PRINTED
C     PRESSURE APPROXIMATION
      IF(J.GT.30) GO TO 912
      IF(EO(47,J).LE.0.0003) GO TO 901
      GO TO 902
 901  IF(EO(47,J) .LT.-0.0003) GO TO 902
      GO TO 903
 903  Z(47,J)=0.0
      DO 600 LM=1,46
      ID=47-LM
      PH=(SIN(TH(ID,J))*EXP(ER(ID,J)))+(SIN(TH(ID+1,J))*EXP(ER(ID+1,J)))
      GF=(RD(ID+1)-RD(ID))
      DH=(1/2.0)*PH*GF
      Z(ID,J)=Z(ID+1,J)+DH
 600  CONTINUE
      COP(1)=0.0
      DO 762 ITT=2,47
      COP(ITT)=RC(ITT,J)/5.0
 762  CONTINUE
      WRITE(3,400)
 400  FORMAT(/////////,T5,'I',T20,'THETA',T35,'INL.RADIUS',T55,'CU.RAD',
     .T75,'SIGMA BAR',T99,'EPSI BAR',T124,'CU.T',////)
      DO 405 I=1,47
      WRITE(3,401)I,TH(I   ,J),ID(I   J),RC(I   ,J),SIGB(I   ,J),EB(I   ,J),
     .T(I   ,J)
```

```
401   FORMAT( /,4X,I3, 6X,F14.7,5X,F14.7,5X,F14.7,5X,F14.7,5X,F14.7,2X,
     .F14.7)
405   CONTINUE
      WRITE(3,402)
402   FORMAT(////,T8,'I',T20,'SIGMA R',T45,'SIGMA O',T60,'EPS.T',T75,
     .'EPS.R',T90,'EPS.THETA',T110,'CO.DIMENLESS.RAD.',////)
      AE(1)=1.0000
      DO 426 I=1,47
      WRITE(3,403)I,SIGR(I   ,J),SIGO(I   ,J),ET(I   ,J),ER(I   ,J),
     .EO(I   ,J),COP(I)
403   FORMAT( /,5X,I3,10X,F14.7,3X,F14.7,3X,F14.7,3X,F14.7,3X,F14.7,3X,
     .F14.7)
426   CONTINUE
      WRITE(3,200)
200   FORMAT(///////,8X,'I,J',10X,'HEIGHT',12X,'RHO1',12X,'RHO2',10X,
     .'T*SIGR/TSIG',////)
      DO 304 I=1,47
      WRITE(3,232)I,J,Z(I,J),RO1(I,J),RO2(I,J),AB(I)
232   FORMAT(/,6X,I3,1X,I3,10X,F14.7,3X,F14.7,3X,F14.7,3X,F14.7)
304   CONTINUE
      WRITE(3,33)J,P(J)
33    FORMAT(//,5X,'CORRECT PRESSURE FOR THE STAGE',I3,10X,F14.7)
      GO TO 35
902   IF(LP.GT.3) GO TO 434
      IF(LP.EQ.3) GO TO 433
      GO TO 435
433   PS(LP)=P(J)
      AC=PS(LP)
      EK(LP)=EO(47,J)
      GO TO 434
435   IF(LP.EQ.2) GO TO 431
      GO TO 434
431   PE=P(J)
      ES=EO(47,J)
      GO TO 434
434   WRITE(3,461)EO(47,J),LP,J,P(J)
461   FORMAT(//,5X,'EEE',F14.7,2I3,F14.7)
C
      IF(LP.GT.3) GO TO 436
      IF(LP.EQ.3) GO TO 433
      GO TO 432
432   P(J)=P(J)+DP
      LP=LP+1
C
C
```

```
      IF(LP.EG.2) GC TO 9
      IF(LP.EG.3) GC TC 9
 438  LP=LP+1
      P(J)=((PS(LP-1)*ES)-(PB*EK(LP-1)))/(ES-EK(LP-1))
C     WRITE(3,445)J,P(J),PS(LP-1),EK(LP-1),PB,ES,LP
C445  FCRMAT(//,5X,I3,5G14.7,5),I3)
      GC TO 9
C436  IF(LP.EG.4.AND.J.EG.12) GO TO 35
 436  PS(LP)=P(J)
      EK(LP)=E0(47,J)
      PS(3)=AC
      P(J)=(PS(LP)*EK(LP-1)-PS(LP-1)*EK(LP))/(EK(LP-1)-EK(LP))
C     WRITE(3,456)J,LP,PS(LP),EK(LP),PS(LP-1),EK(LP-1),P(J)
C456  FCRMAT(//,5X,2I3,5G14.7)
      LP=LP+1
      IF(LP.EG.10) GO TC 459
      GC TO 9
 912  IF(EU(47,J).LE.0.0005) GO TO 915
      P(J)=P(J)+0.50
      GC TO 9
 915  IF(EU(47,J).LT.-0.0005) GO TO 917
      GC TO 903
 917  P(J)=P(J)-0.100
      GO TO 9
C
 35   IF(J.GT.27) DP=0.50
C
 37   CONTINUE
      WRITE(3,749)
 749  FORMAT(///,5X,' J',9X,'PRESSURE', 7X,'POL.THICKNESS',3X,'PCL.TH.ST
     .RAIN',3X,'POLAR CURVATURE',3X,'POL.HOOPSTRESS',5X,'POLAR HEIGHT',
     .3X,'STRESS RATIC.EDGE',///)
      DC 756 J=2,30
      SCFT(J)=SIGO(47,J)/SIGR(47,J)
      WRITE(3,750)J,P(J),T(1,J),ET(1,J),RCI(1,J),SIGR(1,J),Z(1,J),
     .SCFT(J)
```

```
750   FORMAT(/,3X,I3,5X,F14.7,3X,F14.7,3X,F14.7,3X,F14.7,3X,F14.7,3X,
     *F14.7,3X,F14.7)
756   CONTINUE
      WRITE(3,765)
765   FORMAT(///////,30X,'COMPLETE THEORITICAL ANALYSIS FOR SOFT BRASS
     * DIAPHRAGM OF DIAMETER 10 INCHES.')
      WRITE(3,720)
720   FORMAT(/,30X,'*************************************************
     ********************************************')
459   STOP
      END
/*
// EXEC LNKEDT
// EXEC
109240.000        0.510
   67.2606354
  111.9831848
  154.1595306
  194.6531067
  233.4193420
  270.6289063
  307.4108887
  342.4206543
  375.0109863
  405.3452148
  433.4084473
  459.3498535
  483.2998047
  505.2568359
  525.6892090
  544.5048828
  561.7954102
  577.6245117
  592.1215820
  605.3295898
  617.3437500
  628.0480957
  637.8811035
  646.7675781
  654.7377930
  661.8393555
  668.3393555
  673.8393555
  678.7392578
/*
/&
* $$ EOJ
```